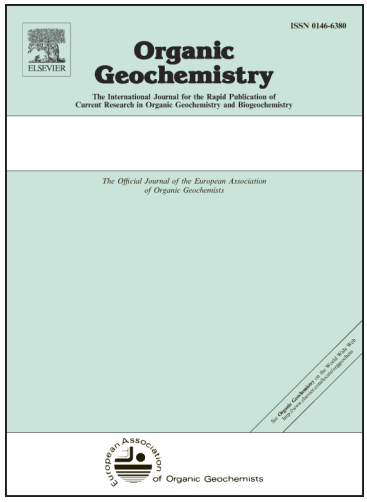

Tropical soil profiles reveal the fate of plant wax biomarkers during soil storage

Mong Sin Wu, A. Joshua West, Sarah J. Feakins

PII: S0146-6380(18)30278-X
DOI: https://doi.org/10.1016/j.orggeochem.2018.12.011
Reference: OG 3827

To appear in: *Organic Geochemistry*

Received Date: 3 July 2018
Revised Date: 7 December 2018
Accepted Date: 24 December 2018

Please cite this article as: Wu, M.S., West, A.J., Feakins, S.J., Tropical soil profiles reveal the fate of plant wax biomarkers during soil storage, *Organic Geochemistry* (2018), doi: https://doi.org/10.1016/j.orggeochem.2018.12.011

Tropical soil profiles reveal the fate of plant wax biomarkers during soil storage

Mong Sin Wu[a], A. Joshua West[a] and Sarah J. Feakins[a*]

[a] Department of Earth Sciences, University of Southern California, Los Angeles, California, USA

[*]Corresponding author: feakins@usc.edu (Feakins)

Highlights:

- Plant wax was studied in soil pits under tropical forests at varied elevation.
- Plant wax concentration and composition were characterized in litter and soil profiles.
- Plant wax D/H invariant within the profiles.
- Significant down-profile ^{13}C-enrichment linked to Suess effect and diagenesis.
- Below-ground plant wax stocks greatly exceed above-ground stocks.

Keywords: soil profile; plant wax; leaf litter; Amazon; Andes; carbon isotope; hydrogen isotope.

Abstract

The waxy coating that protects the leaves and other soft tissues of plants includes *n*-alkane and *n*-alkanoic acid compounds that are commonly used as biomarkers to reconstruct past environment. Plant waxes have geological relevance given their persistence in soils and paleosols, as well as in lake and marine sediments, yet diagenesis may alter their molecular and isotopic signatures from synthesis to deposition. This study seeks to understand the fate of plant wax biomarkers in soils after leaf-fall as characterized by a series of tropical soil profiles. We investigate the changes in abundance, molecular distributions, and hydrogen (δD) and carbon isotopic compositions (δ^{13}C) of plant waxes (*n*-alkanes and *n*-alkanoic acids) in six litter-to-soil profiles along a 2740 m elevation transect from the eastern flank of the Andes mountains down to the lowland Amazon floodplain in Peru. From litter to soil, we find acid/alkane ratios increase, while absolute abundances decrease. In contrast, within each soil, acid/alkane ratios are roughly constant and we find an equivalent exponential decline in concentration in both compound classes with depth; with molecular distributions indicating some new production. We observe a 4 – 6‰ ^{13}C-enrichment from litter to deeper soils for both C_{29} *n*-alkanes and C_{30} *n*-alkanoic acids; of which the Suess effect accounts for ≤ 2‰. We infer that microbial degradation and production (or 'turnover') processes influence the δ^{13}C of plant waxes that survive in soils; in contrast, no systematic change in δD values is observed. The plant wax signal in soils includes averaging of inputs and diagenetic effects, so this signature is particularly relevant for the interpretation of plant waxes archives in paleosols and the plant waxes eroded from soils and exported to downstream sedimentary archives. We show that soils represent the major stock of plant wax under living ecosystems, suggesting that soils may be a quantitatively-important source of plant

37 waxes available for fluvial erosion, with implications for studies of carbon cycling and
38 paleoenvironmental reconstructions from downstream geological archives.

1. Introduction

Plant wax biomarkers are commonly used to reconstruct past environments based upon the carbon and hydrogen isotopic compositions that reflect aspects of vegetation and climate (Eglinton & Eglinton, 2008). Geological applications focus on sedimentary deposits that archive the spatial and temporal record of these molecular fossils, and plant waxes have been found preserved in paleosols (e.g., Magill et al., 2016), lake sediments (e.g., Fornace et al., 2014) and marine sediments (e.g., Tipple and Pagani, 2010). In order to calibrate how the plant wax proxy records aspects of vegetation and climate, many studies have sampled leaves from living vegetation, including studies of temperate forests (Sachse et al., 2006), arid ecosystems (Feakins & Sessions, 2010), tropical forests (Vogts et al., 2009) and high latitude ecosystems (Wilkie et al., 2013). Modern lake sediments (Sachse et al., 2004) and marine core tops (Rommerskirchen et al., 2003) have been used to study plant wax delivered by wind and water transport. Soils have also been surveyed to characterize plant wax variations along altitudinal transects (Jia et al., 2008; Bai et al., 2011), latitudinal transects (Bush and McInerney, 2015; Bakkelund et al., 2018) and aridity gradients (Schwab et al., 2015).

Given the ~2000 Pg of organic carbon stored in soils globally (Batjes, 1996; Jobbágy & Jackson, 2000), soils are a major source of the organic carbon (including plant waxes) eroded from the continents to lake and ocean sediments (Blair et al., 2004). Soils are a particularly important storage step (Blair et al., 2004) between new plant production and erosion by rivers given the age of plant waxes transported by rivers revealed by compound specific radiocarbon (Kusch et al., 2010; French et al., 2018), that suggests storage from decades to thousands of years.

Soils can be sampled as an archive of environmental information *in situ* integrating the time of soil formation, and given requisite burial or protection from erosion soils may be preserved in the form of paleosols, yielding information based on pedogenic structures and thicknesses (e.g., Retallack, 2013) as well as pedogenic carbonate nodules (e.g., Cerling and Quade, 1989, Quade et al., 2013) and more recently plant waxes (e.g. Magill et al., 2016).

When interpreting plant waxes stored in paleosols or derived from soil erosion, we need to understand how plant wax biomarkers are incorporated into soils and how diagenesis may alter their molecular and isotopic signatures from synthesis to deposition. Once a leaf falls from the canopy it forms the litter layer on top of the soil, with leaves comprising the majority, often >60%, of litterfall (Kögel-Knabner & Amelung, 2014). Removal processes associated with herbivory and microbial degradation (and/or runoff erosion on steep slopes) may be considerable, but litter represents the input of organic matter at the top of the soil profile and can contribute to the upward accumulation of soils. In lower layers of the soil, weathering of parent rock may deepen the soil downwards (Amundson, 2014). Over time, soil erosion by water or wind may remove surficial layers of the soil, or landsliding may remove forest, soil and rock such as in the steep-sided Andes (Clark et al., 2016) or the banks of meandering lowland rivers (Torres et al., 2017). The residence time of soil is therefore controlled by the balance of additions from above and below, and removal processes of degradation and erosion (Heimsath et al., 1997). The persistence of soil organic matter, and its individual compounds, is decoupled from the intrinsic thermodynamic stability expected based on molecular structure: many compounds persist decades beyond their expected residence time, reflecting the importance of packaging within soil aggregates and adsorption to minerals (Schmidt et al., 2011). If the persistence of soil organic carbon is an "ecosystem property" (Schmidt et al., 2011), then more work needs to be

done to characterize the fate of individual compounds in a range of ecosystems and terrains for carbon cycle applications, as well as for paleoclimate reconstructions using biomarkers.

1.1 Diagenesis of plant wax biomarkers

Previous research to understand the effect of early diagenesis on plant wax biomarkers has included field studies in low-diversity temperate ecosystems, comparing fresh leaves with litter and soil (Nguyen Tu et al., 2004; Chikaraishi & Naraoka, 2006; Zhang et al., 2017), and monitoring changes with time in litterbag experiments (Huang et al., 1997; Nguyen Tu et al., 2017, 2011; Zech et al., 2011; Wang et al., 2014; Li et al., 2017). Most have studied *n*-alkanes only, with the exception of Chikaraishi & Naraoka (2006) who studied a suite of lipids including *n*-alkanes and *n*-alkanoic acids.

Study of hydrogen isotope effects associated with diagenesis is limited. In a litter bag experiment of three broadleaf tree species, Zech et al. (2011) found seasonal variations of 10 – 20 ‰ in *n*-alkane δD values that were attributed to microbial *n*-alkane production, but they found no systematic overall trend across the 2 year study. In contrast, a study of a soil profile in a Japanese maple forest found D-depletion (by ~50‰) in both *n*-alkanes and *n*-alkanoic acids from leaf to soil, suggesting a significant hydrogen isotope effect during early diagenesis in soils (Chikaraishi & Naraoka, 2006).

In contrast, the carbon isotopic effect associated with plant wax degradation is relatively well-known. Prior studies have reported an increase (~1 – 2‰) in plant wax δ^{13}C during early diagenesis, as reflected in differences between fresh leaves and leaf litter, and also seen in changes during 1-3 yrs of litter decomposition in experiments (Nguyen Tu et al., 2004; Chikaraishi & Naraoka, 2006; Wang et al., 2014; Li et al., 2017; Zhang et al., 2017), although

two shrub species showed no temporal change in $\delta^{13}C$ (Huang et al., 1997; Li et al., 2017). Considering the diversity in species (including maple, ginkgo, bamboo, C3 and C4 grasses, moss) and sites studied so far, a 1 – 2‰ ^{13}C-enrichment appears to be a widespread signature associated with degradation.

1.2 Tropical soils in an Andes-Amazon transect

A litter translocation experiment across the Andes-Amazon transition in Peru has found a strong dependence of litter degradation on soil temperatures, with ~3-fold higher degradation rates at lowland sites of 24°C compared to upland sites of 12°C mean annual soil temperature (Salinas et al., 2010). The dependence of degradation rates on temperature also leads to thicker soils and higher soil organic carbon (OC) contents in the colder montane cloud forests compared to lowland tropical rainforests (Whitaker et al., 2014). Microbial community also changes in response to elevation, with increased microbial biomass and fungi relative to bacteria with increasing altitude, which affects soil respiration rates (Whitaker et al., 2014). These environmental controls and microbial processes not only determine the fate of bulk OC as a whole, but also may have different influence on various types of organic compounds, including plant wax *n*-alkanes and *n*-alkanoic acids.

Here, we study plant waxes in leaf litters and soils from a series of soil pits under tropical forests at contrasting altitudes, spanning sites from the eastern flank of the Peruvian Andes to the Amazon floodplain. We quantify how bulk organic carbon and plant wax molecular and isotopic signatures vary during soil storage by sampling the progression from leaf litter down through the soil profile, with detailed sampling of soil pits dug along the elevation transect across a wide range of temperatures and soil organic layer thickness. We study molecular abundances and C

and H isotope compositions of both *n*-alkanes and *n*-alkanoic acids, aiming towards a more comprehensive understanding of the preservation/alteration of plant wax biomarkers from plants to soils.

This study adds to prior work on plant waxes in the Madre de Dios region of Peru including canopy surveys of leaf wax *n*-alkane molecular abundance distributions and productivity (Feakins et al., 2016a); canopy bulk leaf and leaf wax carbon isotopic composition (Wu et al., 2017); and canopy leaf wax hydrogen isotopic composition together with plant ecohydrology (Feakins et al., 2016b), as well as river export of plant waxes *n*-alkanoic acids related to soil mineral horizon hydrogen isotopic composition (Ponton et al., 2014) and dual isotope comparison of plant wax *n*-alkanes and *n*-alkanoic acids in soils and river (Feakins et al., 2018). Those studies found a linear trend in both $\delta^{13}C$ and δD values of both *n*-alkanes and *n*-alkanoic acids in canopy leaves and soils with elevation, supporting the use of these metrics as proxies for elevation for paleoaltimetry for ancient deposits and to indicate sourcing-elevation of plant waxes exported by rivers within the catchment. The latter study also found an isotopic offset in $\delta^{13}C$ values of the C_{29} *n*-alkane between canopy and soils (Feakins et al., 2018) that we investigate further here.

2. Materials and methods

2.1 Field sampling

We collected samples from four sites across our study area located in the Madre de Dios region of Peru, spanning elevations from 286 m in the Amazon floodplain to 3025 m along the eastern flank of the Andes (Fig. 1, Table 1). The region receives 1560 – 5300 mm mean annual precipitation (MAP) and is fully forested (tropical montane cloud forest to lowland rainforest). The sample sites span a temperature range of 11.1 – 24.4 °C. All sites are primary forests with one secondary growth forest site in the foothills, at Villa Carmen (VC), previously logged and now dominated by bamboos. The primary forest sites are highly-biodiverse. Tree species with high abundance include *Weinmannia crassifolia*, *Clusia alata cf*., and *Hesperomeles ferruginea* at Wayqecha (WAY), as well as *Alchornea latifolia*, *Tachigali setifera*, and *Tapirira obtuse* at San Pedro (SP). The lowland tropical rainforest (TR) is characterized by even higher biodiversity, but abundant Amazonian lineages include *Inga, Swartzia*, *Protieae*, and *Guatteria* including presence of species of those genera at the Los Amigos (LA) site (Dexter et al., 2017). Soil types include Umbrisol at WAY, Cambisol at SP (Whitaker et al., 2014), and Ultisol LA (Pittman et al., 2001), but have not been previously classified at our VC site. Soil organic layer thickness varies from 1 to 26 cm with a tendency towards increasing thickness at higher altitudes (Table 1). Along this transect are a series of permanent forest plots that are part of the Global Ecosystems Monitoring Network (GEM; http://gem.tropicalforests.ox.ac.uk/projects/aberg), where canopy leaf wax has been studied before (Feakins et al., 2016a,b; Wu et al., 2017), and where aggregate soil organic (O) and mineral (M) samples have been collected and studied by amalgamating soils from five locations at each plot (Ponton et al., 2014; Nottingham et al., 2015; Feng et al., 2016; Feakins et al., 2018). Here we study individual vertical soil profiles, sampling

within a single pit to investigate degradation processes and transformation of plant wax signatures during soil storage at each of 4 sites along the elevation transect. Although this region experiences landslides in areas of steep relief (Clark et al., 2016), we selected soil pits at locations where the surface did not appear to be disturbed. Within the soil pits, examination of the color, texture, and structure of the soil profiles suggested that the soils had formed from downward weathering and upward accumulation of leaf litter, without sedimentary structures indicative of disturbance by erosional reworking. At two sites (VC and LA), an additional site was sampled to contrast hillslope setting, by digging one pit at the ridgetop and one at the slope base. In total we present data for 6 pits (Table 1). This soil profile study overlaps with the prior plant wax study of soil O and M layers (Feakins et al., 2018) at WAY and SP where we can make direct comparisons. In addition, we can compare the litter-soil profile at SP with data from canopy leaves from previous studies (Feakins et al., 2016a,b; Wu et al., 2017).

Table 1: Locations and information of sampling sites along the Andes-Amazon transect.

Site name	Site code	Elev (m)	Lat	Long	Temp (°C)	Forest type*	Soil type	Soil pit	Organic layer thickness (cm)	Soil pit depth (cm)	Litter collection
Wayqecha	WAY	3025	-13.1926	-71.5880	11.1	TMCF	Umbrisol	single pit	26	90	Y
San Pedro	SP	1500	-13.0490	-71.5370	18.8	TMCF	Cambisol	single pit	16	40	Y
Villa Carmen	VC	614	-12.8961	-71.4183	22.9	TR	n.a.	ridgetop	5	63	N
								slope base	23	100	Y
Los Amigos	LA	286	-12.5588	-70.0993	24.4	TR	n.a.	ridgetop	1	90	Y
								slope base	13	150	N

* TMCF: tropical montane cloud forest; TR: tropical rainforest. All are primary forests except VC, which is a bamboo-dominated secondary growth forest.

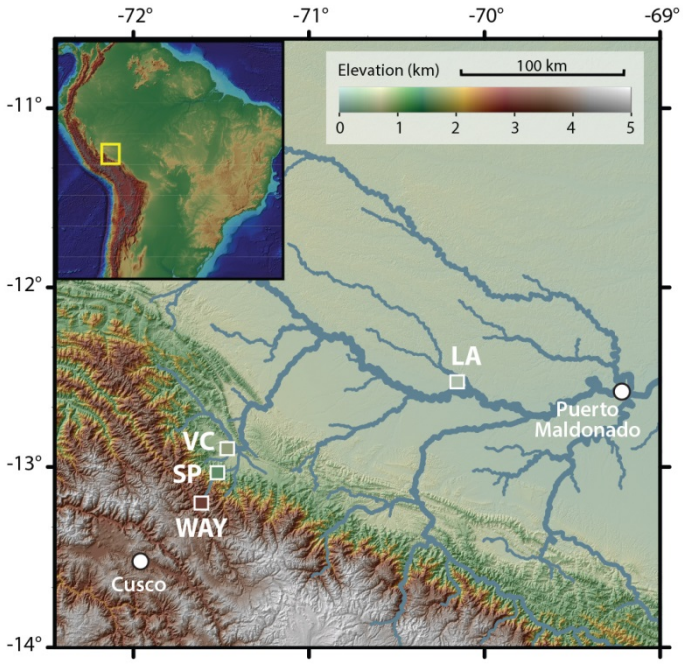

Fig. 1. Sampling locations across a 2740 m elevation Andes-Amazon transect in the Cusco and Madre de Dios region of Peru (square symbols, color indicates elevation). Andean sites: Wayqecha (WAY) and San Pedro (SP). Foothills: Villa Carmen (VC) Lowland: Los Amigos (LA). Circles show major cities in the region.

The two soil profiles at the high elevation sites at Wayqecha (WAY) and San Pedro (SP) are located under tropical montane cloud forest and correspond to the RAINFOR sites of the same names, with the SP site equivalent to RAINFOR SP-1500 (www.rainfor.org). The Villa Carmen

(VC) plot is under a secondary forest in the foothills of Andes, and Los Amigos (LA) is located in the tropical rain forest of the Amazon floodplain. Two soil pits were dug each at VC and LA, with one located at a slope base (VC2 and LA5) and the other located on top of a nearby ridge (VC3 and LA4).

We collected leaf litter at WAY, SP, VC2 and LA4, with the litter at WAY (the upper site) divided into top, middle, and bottom litter because of its thickness (~12 cm). Soil pits were dug to ~90 – 150 cm depth, and 3 – 4 samples (integrating 5 – 50 cm of soil vertically) were taken at each pit based on the soil profile characterization (based on color and physical properties). We also sampled roots at SP and LA4. Samples were stored under cool conditions in the field until transport back to the laboratory where they were stored in a freezer at -20°C, before being freeze-dried. As rock fragments were present in many soil samples, clasts >2 mm were removed by sieving. The soil samples were then ground in a pestle and mortar to homogenize for geochemical analyses.

2.2 Bulk organic carbon analysis

Aliquots of the soil samples were taken for total organic carbon (TOC) and bulk organic carbon isotope ($\delta^{13}C_{OC}$) analysis. The samples were heated in dilute (10%) HCl to 70°C in a water bath for 1 h to remove carbonates. The decarbonated samples were then rinsed three times with deionized water, and dried in an oven at 56°C. The dried samples were analyzed for TOC and $\delta^{13}C_{OC}$ using a Costech Elemental Combustion System (EA 4010) connected via a Picarro Liaison (A0301) to a Picarro cavity ring down spectrometer (G2131-i). A USGS-40 standard (Glutamic Acid with $\delta^{13}C_{OC}$ = -26.6‰ in VPBD scale) was run with replicates at different weights at the beginning and end of the sequence to provide a calibration curve for the measured

209 TOC, as well as an assessment of the precision in $\delta^{13}C_{OC}$ measurements (determined to be better
210 than 0.2‰).

211 2.3 Lipid extraction

212 Total lipid extracts (TLE) were extracted from freeze-dried samples with 9:1 dichloromethane
213 (DCM) to methane (MeOH) using an Accelerated Solvent Extraction system (ASE 350, Dionex)
214 at 100°C and 1500 psi for 2 cycles of 15 mins. The TLE was separated into neutral (FN;
215 containing *n*-alkanes) and acid (FA; containing *n*-alkanoic acids) fractions by eluting 2:1 DCM
216 to isopropanol and 4% formic acid in ethyl ether respectively through a column of LC-NH_2 gel.
217 The *n*-alkanes were then further separated from the FN fraction by eluting with hexane through a
218 silica gel column. The FA fraction was methylated in 5% HCl in MeOH of known isotopic
219 compositions at 70°C overnight, during which the *n*-alkanoic acids were reacted into fatty acid
220 methyl esters (FAMEs). The product was diluted with milliQ water and partitioned in hexane
221 using liquid-liquid extraction. The extract was further separated by eluting through a silica gel
222 column using hexane and DCM, with the DCM fraction carrying the FAMEs.

223 2.4 Compound identification and quantification

224 Samples were dissolved in hexane ready for compound identification and quantification using a
225 gas chromatograph (Agilent 6890) coupled with a mass spectrometer (Agilent 5973) and flame
226 ionization detector (GC-MS/FID). Compound identification was based on retention time and
227 mass spectra of target peaks. Absolute abundance was calculated from peak area response on the
228 FID, based on a calibration curve of an in-house standard mixture of *n*-alkanes and *n*-alkanoic
229 acids of known abundance. We recorded the abundance of *n*-alkanes ($C_{23} - C_{33}$) and *n*-alkanoic
230 acids ($C_{22} - C_{32}$), individual homologues conventionally considered terrestrial plant-derived (G.

Eglinton & Hamilton, 1967), and calculated their total abundance on a μg g^{-1} dry weight basis (∑alk and ∑acid) as well as normalized to TOC, i.e., μg g OC^{-1} (Λalk and Λacid). To represent the molecular distributions of the plant wax homologues, we also calculated the average chain length (ACL) and carbon preference index (CPI) using the following equations:

$$ACL = \sum(n \times [C_n]) / \sum[C_n] \quad \text{(Eq. 1)}$$

$$CPI = 2\,[C_n] / ([C_{n-1}] + [C_{n+1}]) \quad \text{(Eq. 2)}$$

where n indicates the chain length (n = 23 – 33 for *n*-alkanes and n = 22 – 32 for *n*-alkanoic acids), and $[C_n]$ indicates the abundance of that chain length.

2.5 Compound-specific isotopic analysis

The compound-specific carbon and hydrogen isotopic compositions (δD and δ^{13}C) were measured by gas chromatography – isotopic ratio mass spectrometry (GC-IRMS) using a Thermo Scientific Trace gas chromatograph connected to a Delta V Plus mass spectrometer via an Isolink pyrolysis furnace at 1400°C for δD, and a combustion furnace at 1000°C for δ^{13}C. We monitored the linearity of isotopic determinations across 1-7 V peak amplitude daily and only accepted measurements from peaks with amplitude within the range of acceptable linearity. δD and δ^{13}C measurements were normalized to VSMOW/SLAP and VPDB standards respectively, by calibrating against an external standard (A6-mix obtained from A. Schimmelmann, Indiana University) containing a mixture of 15 *n*-alkane compounds ($C_{16} – C_{30}$) with δD and δ^{13}C values ranging from -9 to -263 and -26.2 to -33.8‰ respectively. The isotopic values of *n*-alkanoic acids were then calculated from measured values of FAMEs and known values of the added methyl group by mass balance.

3. Results

3.1 TOC and plant wax abundance

Here we report total abundance of organic carbon (TOC, mass C per gram sediment), and plant wax mid- and long-chain (C_{23-33}) *n*-alkanes and (C_{22-32}) *n*-alkanoic acids normalized to per gram dry sample (∑alk and ∑acid) and per gram OC (Λalk and Λacid) (Fig. 2; Appendix A). TOC ranges from 35.6 – 46.7% in leaf litter, and 0.5 – 19.8% in top soil samples declining to 0.1 – 2% in the deepest soil samples. ∑alk and ∑acid range from 104 – 2279 and 330 – 1200 μg g^{-1} in leaf litter, and from 0.05 – 115 and 0.2 – 603 μg g^{-1} in soil respectively. TOC-normalized Λalk and Λacid range from 248 – 4878 and 786 – 2674 μg g^{-1} in leaf litter, and from 27 – 578 and 170 – 4297 μg g^{-1} in soil respectively. TOC and plant wax abundance varies significantly between sites, and with depth in soils. In general, TOC, *n*-alkanes, and *n*-alkanoic acids trend towards lower abundance with decreasing site elevation, and with increasing depth in each soil profile. At WAY and SP where multiple litter layers were collected, wax abundance shows lower values in the more-degraded litters (lower litter / smaller debris; Fig. 2a,b). In roots, ∑alk and ∑acid range from 0.6 – 5.1 and 42 – 55 μg g^{-1} respectively, which represent <0.6% and <16% of the abundance found in leaf litter. While *n*-alkane and *n*-alkanoic acid abundance both decrease from top to bottom in each profile, the ratio of relative abundance between the two compounds classes exhibits a vertical trend; the fraction of *n*-alkanoic acid, *F*acid = ∑acid/(∑alk+∑acid), shows increasing values from litter (ranging 0.2 – 0.8) to soil (generally >0.8). Furthermore, Λalk decreases from litter to top soil whereas Λacid generally increases for all four litter-soil profiles in this study. These trends indicate an increase in abundance of *n*-alkanoic acids relative to *n*-alkanes from litter to soil.

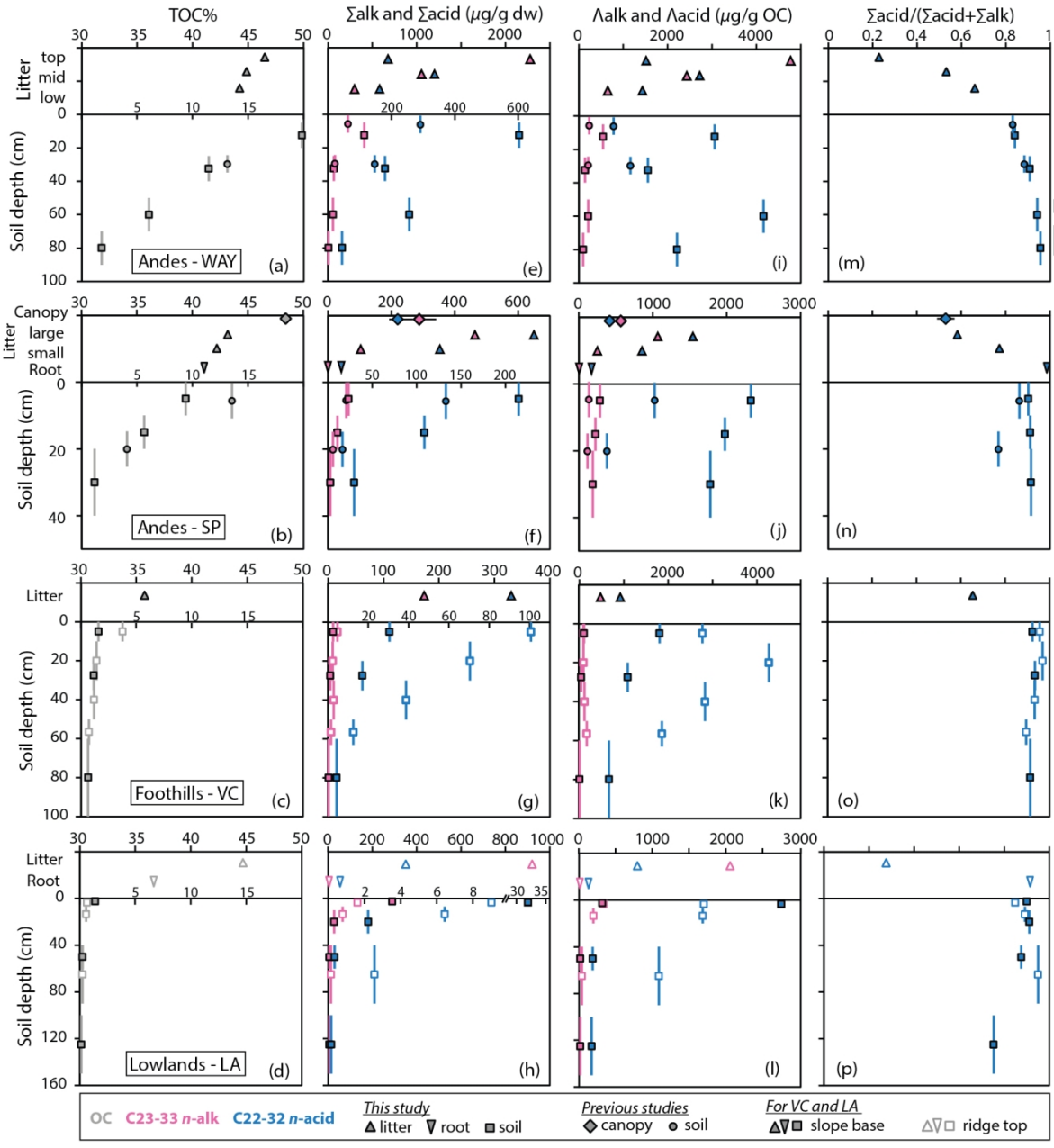

Fig. 2. Vertical profiles of plant wax and bulk OC abundance at the four study sites (pink: $C_{23\text{-}33}$ *n*-alkanes; blue: $C_{22\text{-}32}$ *n*-alkanoic acids), showing (a-d) total organic carbon concentrations, (e-h) abundance per gram dry weight (∑alk and ∑acid), (i-l) abundance normalized to OC (Λalk and Λacid), (m-p) *n*-alkanoic acid fraction. Data shown are from this study (litter: triangle; root: inverted triangle; soil: square), as well as from previous studies (canopy: diamond; soil: circle) of overlapping sites at WAY and SP (Feakins et al. 2016a,b; Feakins et al., 2018). Open symbols at LA and VC denote additional pits at these sites at the ridge top, with closed symbols representing slope base. Vertical bars indicate the depth range from which the soil profile samples were taken. Horizontal bars of canopy data at SP represent standard error of the site means (n = 39). Note the change in x-axes for soil data on the left panels.

3.2 Chain length distributions

In litter and soil, *n*-alkanes show a strong odd-over-even preference from C_{23} – C_{33}, with C_{29} and C_{31} being the dominant compounds, trending towards higher C_{31}/C_{29} ratio in the lower-elevation sites (Fig. 3, left). From litter to soil, we observe a general increase in the mid-chains ($C_{23\text{-}27}$) leading to lower relative abundance of C_{29} and C_{31}. The two root samples have different chain length distributions of *n*-alkanes, with the sample from SP showing similar distributions to that of litter and soil (C_{29} and C_{31} dominating with low $C_{23\text{-}27}$; Fig. 3c), while the sample from LA shows exceptionally high C_{23} and C_{25} that is distinct from litter and soil distributions at this site (Fig. 3g).

n-Alkanoic acids exhibit an even-over-odd preference from C_{22} – C_{32}, with C_{30} or C_{32} being the dominant compound in litter, whereas soil shows a more 'flat' distribution across chain lengths owing to an increase in the abundance of mid-chains $C_{22\text{-}26}$ (Fig. 3). Similar to *n*-alkanes, we also observe a trend towards longer chain lengths (higher C_{32}/C_{30} ratio) towards lower-elevation sites. Roots show distinctively different distributions with dominance by mid-chains in both sites (Fig. 3d,h).

Carbon preference index (CPI) and average chain length (ACL) calculations provide more quantitative comparisons of molecular distributions between samples (Fig. 4). We find that CPI of *n*-alkanes exhibits a wide range from ~4 – 16, with decreasing values from litter to soil at all sites. Lower *n*-alkane CPI values are found in roots (CPI = 4.1–7.1) compared to litter (CPI = 6.6–16.1). In contrast, CPI of *n*-alkanoic acids shows a relatively invariant vertical profile among litter, roots, and soil, with only the top litter at WAY and the canopy leaves at SP being exceptions with slightly elevated CPI.

ACL of both *n*-alkanes and *n*-alkanoic acids shows a decrease (by *c*.1) from litter to soil at WAY, VC and LA, but a relatively straight profile at SP. Litter shows a trend towards higher ACL at lower-elevation sites. Roots exhibit lower ACL compared to litter and soil, related to high abundance of mid-chain length compounds (Fig. 3). Overall, the soil CPI and ACL results from this study match well with data from previous soil studies (Fig. 4 circles; Feakins et al. 2016a,b; Feakins et al., 2018) at WAY and SP.

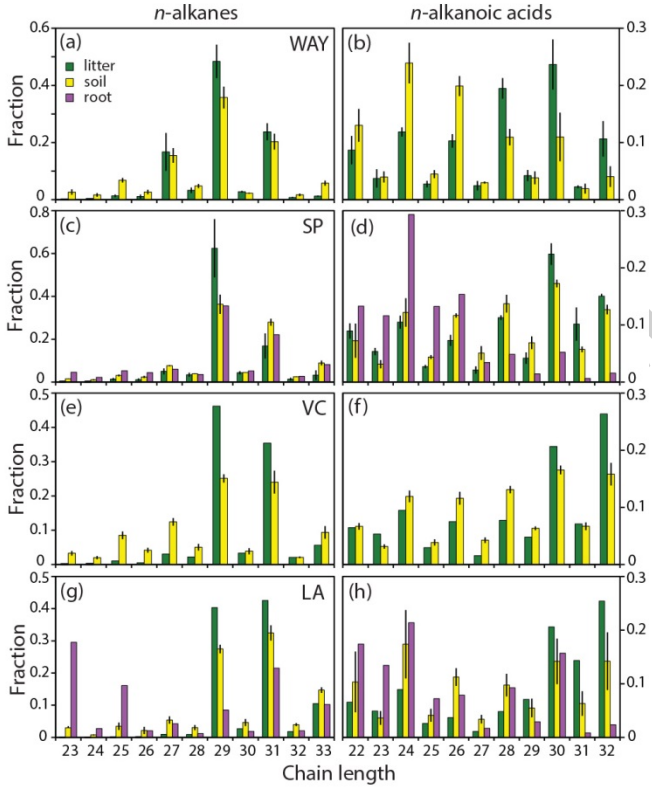

Fig. 3. Chain length distributions of *n*-alkanes (left) and *n*-alkanoic acids (right) in litter (green), soil (yellow), and roots (purple) at the four study sites. Error bars represent 1σ deviation from the mean values when multiple litter or soil samples are present at a single site.

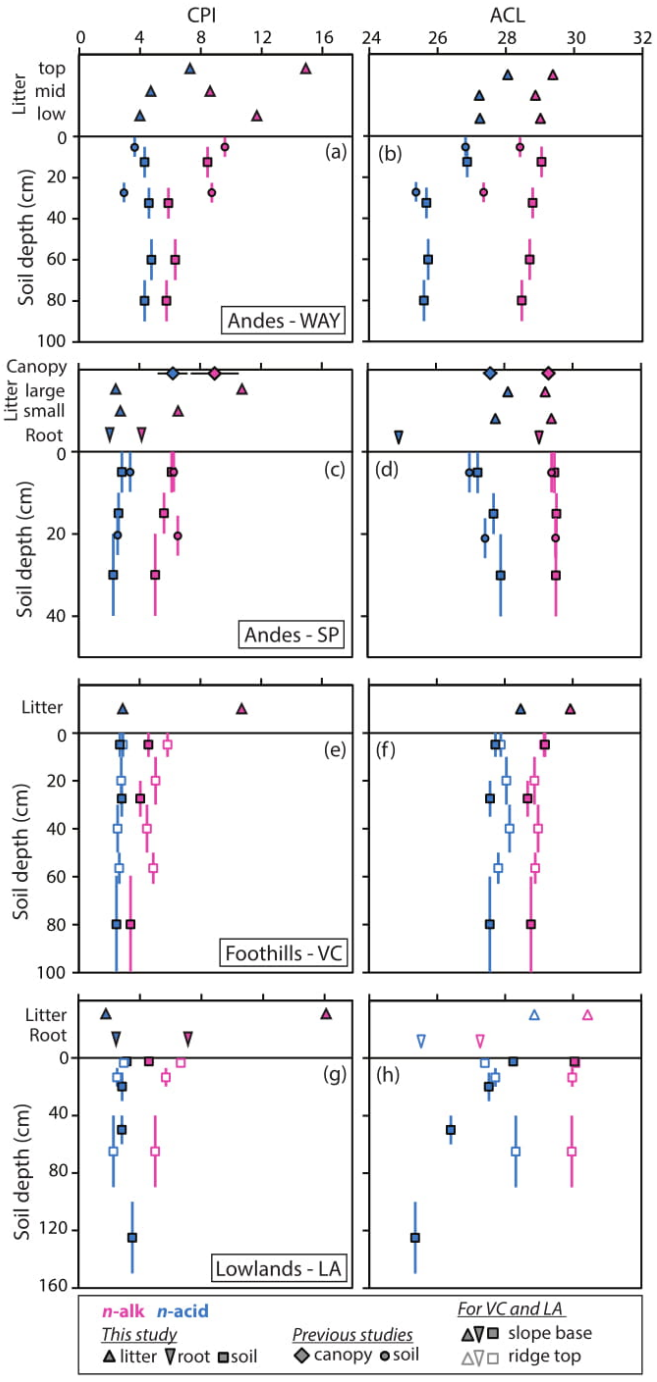

Fig. 4. Vertical profiles of (left) carbon preference index (CPI) and (right) average chain length (ACL) of $C_{23\text{-}33}$ *n*-alkanes (pink) and $C_{22\text{-}32}$ *n*-alkanoic acids (blue) at the four study sites, showing data from this study (litter: triangle; roots: inverted triangle; soil: square). Open symbols at LA and VC denote additional pits at these sites at the ridge top, with closed symbols representing slope base. Also shown are canopy (diamond) and soil (circle) data from previous studies of overlapping sites at WAY and SP (Feakins et al. 2016a,b; Feakins et al., 2018). Vertical bars indicate the depth range from which the soil profile samples were taken. Horizontal error bars of canopy data at SP represent standard error of the site means (n = 39).

3.3 Hydrogen and carbon isotopic compositions

We report δD and δ^{13}C values of $C_{27\text{-}31}$ odd-chain *n*-alkanes and $C_{22\text{-}32}$ even-chain *n*-alkanoic acids when reliable isotopic measurements could be made on these samples (Appendix A). We focus our attention on the most dominant chain length of each compound class, C_{29} *n*-alkane and C_{30} *n*-alkanoic acid. Although we do not show data from all the chain lengths on Fig. 5, the general isotopic patterns described below are shared among the homologues of each compound class, as reported in Appendix A. We also report bulk $\delta^{13}C_{OC}$ values to compare with the plant wax data.

The hydrogen isotopic composition of C_{29} *n*-alkane (δD_{29alk}) and C_{30} *n*-alkanoic acid (δD_{30acid}) ranges from -173 to -210‰ and -158 to -207‰ respectively across all sites, with a general trend towards more enriched values at lower-elevation sites (Fig. 5). C_{30} *n*-alkanoic acid is generally about 5 – 20‰ enriched relative to C_{29} *n*-alkane in the same samples. Both δD_{29alk} and δD_{30acid} show relatively small (<20‰) variations within the soil profiles. However we see no systematic patterns in δD with depth across the four sites: a 5 – 20‰ decreasing trend at WAY and VC slope base for C_{29} *n*-alkane, and at WAY, SP, VC slope base and LA ridge top for C_{30} *n*-alkanoic acid; a ~5‰ increase for C_{30} *n*-alkanoic acid at LA slope base; a ~10‰ increase towards ~40cm depth followed by a 5‰ decrease below at VC ridgetop for both compounds; and no trend for C_{29} *n*-alkane at SP and LA (Fig. 5). We find a much depleted δD_{30acid} value (-206‰) for the root sample from LA compared to soil at this site (ranging ~160 – 170‰), though abundance of C_{29} *n*-alkane was insufficient for δD analysis. For the root sample from SP (10 – 20g mass), neither compound was sufficiently abundant for δD analysis.

The carbon isotopic compositions of C_{29} *n*-alkane ($\delta^{13}C_{29alk}$), C_{30} *n*-alkanoic acid ($\delta^{13}C_{30acid}$), and bulk OC ($\delta^{13}C_{bulk}$) range from -32.4 to -42.9‰, -31.5 to -40.4‰, and -24.5 to –33‰ respectively across all sites (Fig. 5). C_{29} *n*-alkanes are depleted relative to C_{30} *n*-alkanoic acids (by ~2‰) which are in turn depleted by ~6‰ from bulk OC in the same samples. We find consistent patterns of $\delta^{13}C$ with depth for bulk OC and both plant wax compounds across all four sites: a trend of *c*. 4 – 6‰ enrichment from litter to soil at depth, which is a combination of *c*. 2 – 4‰ enrichment between litter and top-layer soil, and *c*. 2‰ gradual enrichment down the soil profile (Fig. 5). Roots yield $\delta^{13}C$ values that are similar to litter or top-layer soil but more depleted than soils at depth (Fig. 5f,h). Across the elevation transect, we find a general trend towards more depleted $\delta^{13}C$ values in lower-elevation sites.

When comparing soil data from this study (Fig. 5, squares) to that at WAY and SP from previous studies (Fig. 5, circles; data from Feakins et al., 2018) in which isotopic data were measured at two depth ranges (organic and mineral horizons), we find results are consistent, with both sets of data showing no systematic patterns in δD with depth, and a ^{13}C-enrichment in the deeper soil. We find the vertical profiles of δD (no consistent trend) and $\delta^{13}C$ (deeper layers are more enriched) are consistent among all chain lengths of *n*-alkanes and *n*-alkanoic acids (Appendix A).

3.3.1 Slope base-ridgetop comparisons

We contrasted slope base and ridgetop settings by digging two soil pits each at VC and LA, to reveal possible difference at locations that are less well-drained with thicker O-layer (slope base) and more well-drained with thin O-layer (ridgetop). While *n*-alkane δD at LA has limited data to allow comparison, we find that in general, the ridgetop shows enrichment in both H (by ~10–20‰) and C (by ~1–3‰) isotopes relative to slope base. At VC, while the uppermost soil

370 samples show similar δD and δ^{13}C values, the ridgetop location appears to be more enriched in
371 both isotopes at deeper depths. At LA, there is consistently isotopic enrichment from the top soil
372 to deeper soil.

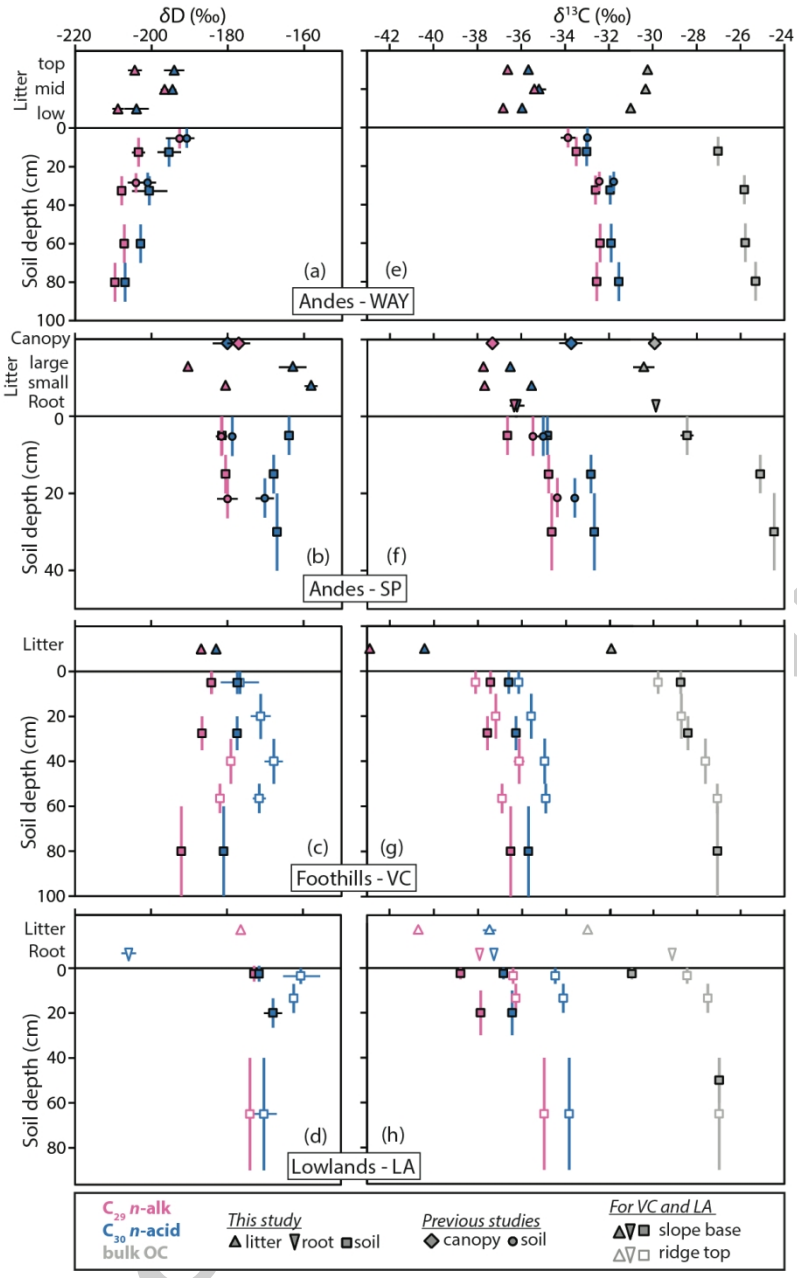

Fig. 5. Vertical profiles of (left, a-d) δD and (right, e-h) δ^{13}C of C_{29} *n*-alkane (pink), C_{30} *n*-alkanoic acid (blue), and bulk OC (grey) at the four study sites, showing data from this study (litter: triangle; root: inverted triangle; soil: square). Open symbols at LA and VC denote additional pits at these sites at the ridge top, with closed symbols representing slope base. Also shown are canopy (diamond) and soil (circle) data from previous studies of overlapping sites at WAY and SP (Feakins et al. 2016a; Wu et al. 2017; Feakins et al., 2018) for comparison. Vertical bars indicate the depth range from which the soil profile samples were taken. Horizontal bars indicate 1σ error from replicate measurements (for soil and litter data) or standard errors of site mean (canopy data at SP).

4. Discussions

4.1 Alteration of plant wax signatures across the litter-soil profile

Numerous plant-based surveys have characterized how plant waxes record environmental variables, providing a basis for interpreting the chemical fingerprints in these biomarkers as climate proxies in sedimentary archives. But an unresolved question relates to possible changes in plant wax signatures between plant and sediment which may compromise the environmental information they carry. In this section, we evaluate the changes observed in abundance, molecular distributions, and isotopic compositions of plant wax from litter to soil in the Peru transect studied here, and we discuss the processes that may lead to these changes.

4.1.1 Plant wax transformation within leaf litter

Sampling of thick leaf litter accumulations at WAY and SP reveals substantial loss of plant waxes within the leaf litter, in contrast to a limited OC loss (~2 – 5%). We find a decrease in concentrations (in terms of both per gram dry weight and OC-normalized) by ~77 – 87% for *n*-alkanes and ~10 – 45% for *n*-alkanoic acids between top litter (large litter) and bottom litter (litter debris) at both sites. We note that there is an increase in ∑acid in the middle litter layer at WAY, which may imply new additions (perhaps by microbial productions during litter diagenesis) or simply heterogeneity within the coarse debris. The overall significant decrease in *n*-alkane abundance within litter suggests rapid degradation of these molecules during early diagenesis. Such rapid loss via degradation has also been observed from litterbag experiments that show >80% loss of plant waxes within 1-3 years, as a result of microbial degradation and perhaps also consumption by herbivores such as mesofauna (Zech et al., 2011; Li et al., 2017; Nguyen Tu et al., 2011, 2017). Our field data corroborate these experimental observations.

Although both compound classes lose concentrations within litter, there appears a better preservation for *n*-alkanoic acids, as shown by an increase of their abundance relative to *n*-alkanes from top (large) to lower (small) litter at WAY and SP (Fig. 2i-l). The better preservation for *n*-alkanoic acids is also evidenced by generally higher litter-to-soil Λacid in contrast to the decrease in Λalk, indicating a greater portion of *n*-alkanoic acids survive litter degradation and enter the soil (Fig. 2e-h). It is unclear why *n*-alkanes may be lost at a faster rate than *n*-alkanoic acids during litter decomposition; this phenomenon has not been observed in the previous leaf litterbag studies which lack the compound class comparison. We speculate that a different rate of loss between the two compound classes is possible if they are not homogenous on the leaf surface, such as if they exhibit different morphological structures, and if *n*-alkanes dominate the more fragile surface wax crystals whereas *n*-alkanoic acids form the lower wax layers. For example, under scanning electron microscopy of plant leaves of other species, $C_{24\text{-}30}$ *n*-alkanoic acids are observed to form smooth wax films, whereas $C_{29\text{-}31}$ *n*-alkanes form various wax types including films, crust, and ridged rodlets (Koch et al., 2009), with crystal structures that extrude from the surface and hence may be more easily lost. Though the exact mechanism unclear, the observation that *n*-alkanes are preferentially lost within leaf litter bridges the discrepancy in the relative concentrations of these two compounds between canopy leaves and soils: canopy leaves commonly contain more *n*-alkanes than *n*-alkanoic acids (abundance data from Feakins et al., 2016b, Wu et al., 2017) whereas *n*-alkanoic acids dominate in soils and river suspended sediments (abundance data from Feakins et al., 2018).

4.1.2 Exponential decline of plant wax concentrations with depth in soils

Below the litter layer, we find further significant drop in plant wax concentrations in soils with depth (by ~65 – 99% from top soil to 50 cm depth for both compounds, similar to the decline in

TOC by ~57 – 90% from top to 50 cm; Fig. 2). Since the absolute concentrations at different sites significantly vary, in order to compare sites, we first calculated fractional concentrations relative to the top sample (within O horizon) at each site, and then characterized the rate of loss (k_z; depth-dependent decay rate) by fitting an exponential decay function. We find exponential loss in concentrations in soils with k_z ranging from 2.1±0.9 to 6.2±1.4 m^{-1} for OC, from 2.3±0.6 to 16.1±1.2 m^{-1} for *n*-alkanes, and from 2.9±0.3 to 15.2±0.7 m^{-1} for *n*-alkanoic acids (Fig. 6).

In contrast to the greater loss of *n*-alkanes relative to *n*-alkanoic acids observed in litter as described in section 4.1.1, the two compound classes appear to drop in concentration with depth at the same rate (no significant difference in k_z values) except at WAY where the k_z value of *n*-alkanes is about double that of *n*-alkanoic acids. This distinction between plant wax loss in litter and within soil profiles soil implies different mechanisms governing the resilience of plant waxes in litter vs. soils. Within soils, physical protection in soil aggregates and absorption to soil minerals is known to play an important role in the stability of soil organic matter (Schmidt et al., 2011). Previous soil studies have found turnover times for both *n*-alkanes and *n*-alkanoic acids also to be similar and on the order of several decades (Wiesenberg et al. 2004; Schmidt et al., 2011).

We cannot infer turnover times from the k_z values calculated based on the decreases in concentration within depth in our soil profiles, because we lack chronological information for the soils in this study. Further, we note that the exponential decline in concentrations with depth observed in this study may be affected by downward mobilization in addition to decomposition, although downward transport would not be expected to produce a carbon isotope fractionation with depth. Overall, the exponential decrease in plant wax concentrations is probably determined

450 by a combination of accumulation of plant wax inputs on the soil top, downward-transportation
451 by mesofauna such as earthworms (Oades et al., 1993) and decomposition of plant waxes within
452 the soil over time.

453

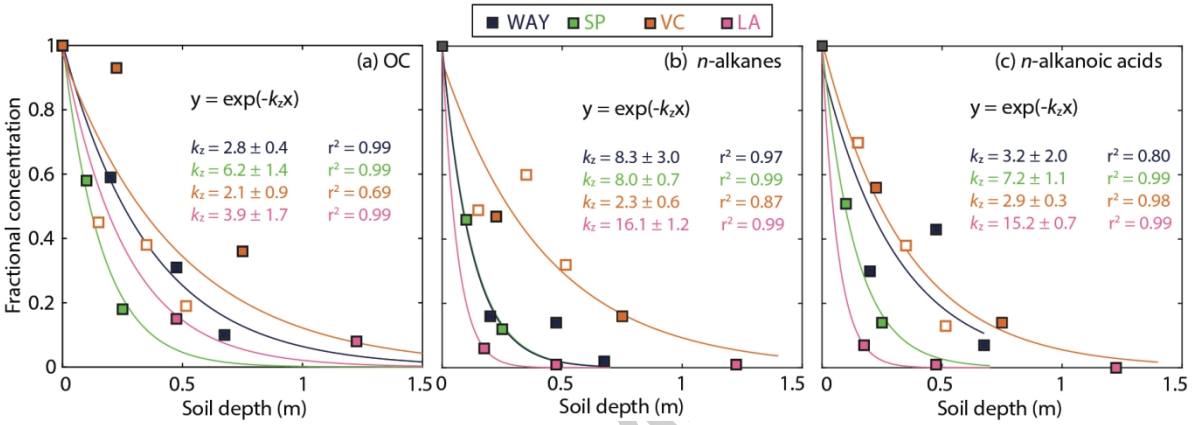

454

455 Fig. 6. Exponential decrease in the total abundance of (a) bulk OC, (b) *n*-alkanes (C_{23-33}), and (c) *n*-alkanoic acids
456 (C_{22-32}) within soils profiles at the four sites. Data show fractional concentrations relative to the top soil samples at
457 each site. Soil data are plotted on the mean sample depth below the top sample. Depth-dependent rate constants (k_z)
458 are estimated with 1σ uncertainties, which show the same values within uncertainties among compounds, except at
459 for *n*-alkanes WAY and bulk OC at LA. Soil profiles at ridgetop (open symbol) and slope base (solid symbol) at VC
460 are grouped for curve fitting. Note that the ridgetop soil pit at LA is excluded in this analysis due to the very thin
461 soil O layer (1 cm) at much finer resolution than the top sample (0-7 cm).

462 Across the four sites, we observe up to six-fold difference in the rate of loss with soil depth, with
463 increase in k_z values from VC, to WAY, SP and LA (except for OC at LA). What determines the
464 difference among sites? The tendency is for an increase in k_z as elevation decreases and
465 temperature increases, which is a known factor for determining rates of respiration. Across the
466 same Andes-Amazon transect, a litterbag translocation experiment which tracked litter
467 decomposition of 15 species over 1.2 yr (Salinas et al., 2010) found that while species type has a
468 large influence on the decomposition rate (k), soil temperature stands out as the main control
469 when averaging all species, such that a five-fold increase in the k value is observed from the high

Andes (WAY at 3025 m, 11.1°C) to the lowland Amazon (Tambopata at 210 m, 23.9°C; similar elevation to LA site in this study). This temperature-sensitivity for litter decomposition rates (k; Salinas et al., 2010) is reflected in the different k_z values of plant waxes at WAY, SP and LA (Fig. 7), which increase progressively from high to low elevation, implying that temperature may also be the main control on the rate of plant wax loss. The k_z values of OC at WAY and SP also follow the same trend as plant waxes, but the apparent lower rate of OC loss at LA is surprising (Fig. 6a; Fig. 7). It is possible that the OC left in these deeper soils at LA is relatively recalcitrant, if the majority of labile OC have already been degraded near the top of the soil due to the warm temperature at this site. This change in recalcitrance would not be expected to be seen in the plant waxes, perhaps explaining with the trends in k_z for waxes are more systematically related to temperature than bulk OK. Overall, we infer that temperature is a primary control on the rate of decline of plant wax concentration and that decomposition likely dominates the depth-decay of plant wax concentration profiles.

An exception to the overall temperature trend for the k_z of the plant waxes is found at VC, which shows much slower loss (lower k_z) than predicted for its elevation (Fig. 7). We note that while the other three sites are in primary tropical forests, VC is in a secondary forest previously logged for timber (Table 1), with secondary-growth bamboos dominating the canopy. Bamboos are known as one of the fastest growing plants on earth, with relatively slow litter decomposition rates (Liu et al., 2010) partly due to the abundance of phytoliths (Piperno and Pearsall, 1998), hence having significant implications for carbon accumulation and storage in soils (Zhou et al., 2005). However, little plant wax research has been done on bamboo leaves (Li et al., 2012, 2016), and the preservation of plant waxes in soils of bamboo forests remains unknown. Here, we find a lower than expected k_z which may imply a greater accumulation of soil organic matter

493 in this presently bamboo-dominated forest, or some other aspect of the landscape disturbance,
494 such as any use of fire which may add to soil organic carbon and slow decomposition. This
495 exception is a useful reminder that while temperature may be a major control on the rate of
496 organic carbon and plant wax loss in well-drained soils, other factors like waterlogging,
497 disturbance and species succession may also modify soil organic properties.

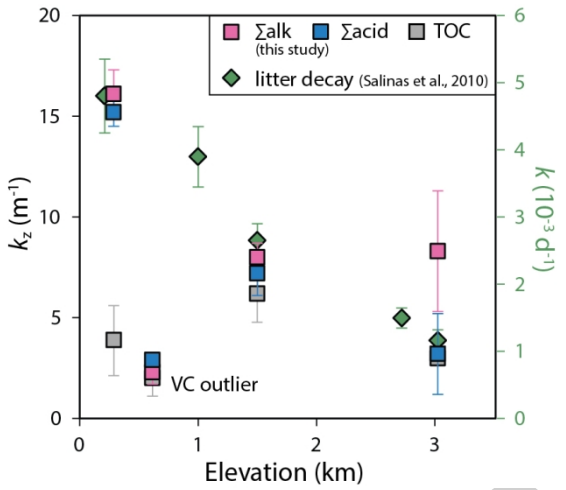

498

499 Fig. 7. The rate of OC and plant wax loss with soil depth (k_z; this study) and litter decomposition rate (k; Salinas et
500 al., 2010) along the Andes-Amazon elevation transect. Note that the soil under secondary growth at VC is an outlier
501 that does not follow the temperature-dependency of k_z values. Litter bag experiments were not conducted at the
502 secondary forest sites at VC. The lower than expected k_z value for bulk OC at LA (the lowest elevation site) may be
503 in part explained by the recalcitrance of residual bulk organic material at depth in these soils.

504 #### 4.1.3 The role of microbial activities in plant wax degradation in soils

505 Microbial activities are prevalent in the tropical soils along the Andes-Amazon transect, and
506 prior studies found them to be critical in soil carbon cycling processes (Whitaker et al., 2014).
507 The degradation and alteration of plant waxes in the soils studied here is likely also significantly
508 governed by soil microbial activities. Laboratory-based experiments have provided direct
509 evidence for microbial activity increasing alongside plant wax decay. During a 3-year room-
510 condition soil storage experiment, Brittingham et al. (2017) found increased genes linked to *n*-

alkane degrading enzymes, alongside a loss of long-chain (C_{29-31}) and rise in shorter-chain (C_{21-25}) *n*-alkane relative abundance, indicating microbial reworking of long-chain into mid-chain homologues. This change in the molecular distribution was also marked by decreased ACL and CPI in the experiments. In line with those experimental results, an increase in mid-chain (C_{23-25}) *n*-alkanes relative to total (Fig. 8), together with a decrease in CPI (Fig. 4), is apparent down profile in our study, consistent with the occurrence of microbial degradation of *n*-alkanes. The soil profiles suggest that microbial degradation affects plant waxes from the very earliest stages of diagenesis; for example the biggest drop in *n*-alkane CPI happens at the litter-soil interface (Fig. 4).

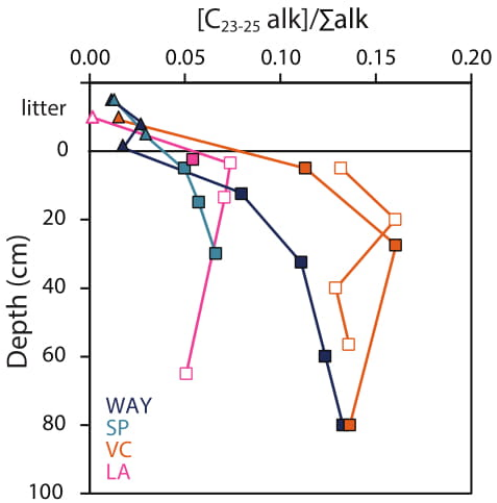

Fig. 8. Increase in mid-chain (C_{23-25}) *n*-alkane fractional abundance down the litter-soil profiles, showing data from litter (triangles) and soils (squares) from the four sites. Note that both ridgetop (open symbols) and slope base (solid symbols) pits are shown for VC and LA. We find no such consistent increase in mid-chain proportions for *n*-alkanoic acids across the sites.

Apart from degradation, microbial activities can also affect plant wax signatures by contributing *n*-alkanes and *n*-alkanoic acids to the soil pool. Though commonly assumed to be dominated by terrestrial vascular plant sources in paleo reconstructions, long-chain *n*-alkanes (>C_{27}) and *n*-

alkanoic acids (>C_{28}) could also be produced by microbes as previous studies have shown (Nguyen Tu et al., 2011; Summons et al., 2013; Makou et al., 2018). It is possible that both degradation and addition of these compound classes may occur in soils, and this can be detected by examination of molecular abundance distributions. In a 1.5-year soil incubation experiment, researchers detected microbial production of long-chain (C_{27-31}) *n*-alkanes with an estimated turnover rate of ~0.1% per year (for *n*-C_{29}) under aerobic conditions, though no significant production was detected under anaerobic conditions (Li et al., 2018). *n*-Alkane-degrading microbes can convert these molecules into *n*-alkanoic acids following identified aerobic and anaerobic degradation pathways involving alkane hydroxylases (Ji et al., 2013), leading to accumulation of *n*-alkanoic acids relative to *n*-alkanes, which is favored in soils with low pH ~3.8 as observed in a soil experiment, whereas higher pH ~7.3 favors higher abundance of *n*-alkanes (Bull et al., 2000). We note that soils throughout the Peruvian Andes-Amazon transect have low pH values ~4 (Whitaker et al., 2014), which based on these experimental results may enhance the accumulation of *n*-alkanoic acids relative to *n*-alkanes as we see in our soils (Fig. 2).

4.1.4 Are root and fungal contributions of plant waxes significant?

Root-derived organic carbon (OC) represents a significant source of soil organic matter, in part due to enhanced protection mechanisms of root-derived versus shoot-derived OC in soils, e.g. as root-hairs can burrow inside of soil aggregates providing physical protection of root-derived OC (Rasse et al., 2005). In terms of plant waxes, grass roots have been found to produce long-chain *n*-alkanes with high odd-over-even preference and C_{31} dominance (Marseille et al., 1999), as well as *n*-alkanoic acids with a distinct chain length distribution (C_{22-24} dominance) compared to leaves and stems (C_{28} and C_{30} dominance) (Wiesenberg et al., 2012). From a litter-soil profile in

550 a grass-dominated landscape, Naafs et al. (2004) deduced substantial root input of lipids,
551 including long-chain *n*-alkanes and *n*-alkanoic acids, into soils. It is unclear how much roots
552 contribute to plant waxes in soils in natural tropical forests such as in our study area, as such data
553 are lacking perhaps in part due to the difficulties in field collection and identification of
554 entangled roots from diverse tree species, especially in the context of very high biodiversity in
555 the western Amazon and Andes (Silman, 2014). However, given the anatomy of plants, root-
556 derived OC is presumably less important in forests than in grasslands (Oades, 1993), given the
557 higher above-ground biomass of trees relative to grasses.

558 Although we only have studied two available root samples from SP and LA, the results provide
559 some clues to whether root inputs of *n*-alkanes and *n*-alkanoic acids are important in these soils.
560 These two roots show very low plant wax abundance, with <1% *n*-alkane and 6-16% *n*-alkanoic
561 acid concentrations compared to litter (Fig. 2b,d). Given the lower net primary productivity
562 allocated to roots than canopy across the same Andean transect (Malhi et al., 2016), a low plant
563 wax concentration in roots suggests a tiny root contribution to soil on a biomass basis, although
564 these may be overrepresented given the greater preservation potential previously noted. Another
565 line of evidence comes from the molecular distributions. If plant waxes in soils are mainly
566 derived from roots, we would expect to see molecular distributions in soils that are more similar
567 to roots compared to leaf litter. While the *n*-alkane molecular distributions are similar between
568 litter and roots at SP (Fig. 3c), confounding any separation on this basis, the molecular
569 distributions of *n*-alkanes at LA (Fig. 3g) and *n*-alkanoic acids at both SP and LA (Fig. 3d,h) are
570 distinct in roots versus litter. In general, we do not find evidence of significant root inputs of *n*-
571 alkanes and *n*-alkanoic acids, as soils show more similar molecular distributions to that of litter
572 (C_{29} and C_{31} *n*-alkane, and C_{30} and C_{32} *n*-alkanoic acid dominance), and lack the distinct

signatures shown in roots (C_{23} and C_{25} *n*-alkane dominance at LA, $C_{22\text{-}26}$ *n*-alkanoic acid dominance with low even-over-odd preference in that range). Moreover, the one available δD measurement of root *n*-alkanoic acid at LA is significantly D-depleted (by ~40‰) relative to the adjacent soil profile (Fig. 5d), further supporting a minor influence of root inputs to soil plant waxes.

Fungi have been reported to contain *n*-alkanes often with C_{27}, C_{29} and C_{31} dominance similar to that of vascular plants (Weete, 1972), but not long-chain (>C_{28}) *n*-alkanoic acids (Weete, 1972; Madan et al., 2002). Other studies have found increases in C_{25} and C_{27} *n*-alkanes in sub-surface horizons and attributed these to fungal production (Huang et al., 1996; Marseille et al., 1999). It may be difficult to use *n*-alkane molecular distributions to detect fungal inputs given the wide diversity of fungi, poor characterization of *n*-alkane production (only few species characterized), and possible confounded distributions with vascular plants (Weete, 1972). A sub-surface increase in abundance of total *n*-alkanes or particular chain lengths such as C_{27} is expected if fungal input is substantial as in previous reports (Huang et al., 1996; Marseille et al., 1999), and we do not observe any such feature in our profiles. However, we note that in those prior fungal studies, the sub-surface increase in fungal *n*-alkanes occurs within a discrete, thin layer a few to ten centimeters down from soil tops, perhaps guided by visual evidence during sampling. If any fungal *n*-alkane production happens at such shallow depth within our soils, this production would not be observed by our relatively coarse profile sampling, and no fungal evidence was observed in the field.

4.1.5 No systematic change in plant wax δD between canopy, litter and soil

The hydrogen isotopic compositions of both C_{29} *n*-alkane and C_{30} *n*-alkanoic acid (the dominant chain length of each compound class) show minor variations (<20‰) down profile with no systematic pattern observed across sites (Fig. 5). The lack of systematic trend in plant wax δD values within the litter layer and soil profiles in this study means we have no evidence for any isotopic effect, whether via new inputs or below ground processes such as degradation and remobilization, during soil formation. One possibility is that downward-transport of plant waxes (such as by mesofauna), may have homogenized plant wax characteristics; however the different patterns of δD and δ^{13}C values with depth, measured on the same molecules, do not support mixing as a major process for these soils. Concentration data have been interpreted as indicating microbial decomposition within litter and soil during the timescales of soil formation. As we do not find a systematic change in δD values, we infer no evidence for any consistent hydrogen isotope fractionation effects associated with early diagenesis here.

This interpretation is consistent with a 27-month litterbag degradation study conducted on three higher plant species in a German spruce forest (Zech et al., 2011). In that study, researchers found no overall trend in $C_{27\text{-}31}$ *n*-alkane δD over the course of the study. They suggested minor (~10 – 20‰) fluctuations were linked to seasonal variations of soil water δD on the microbial community, but no systematic change in *n*-alkane δD was observed in their 2-year litterbag experiment. Our study extends from leaf litter to consider the soil profile and finds that there is no change in plant wax δD during the timescale of soil formation in this system.

In contrast, a leaf-litter-soil profile in a maple forest in Japan (Chikaraishi & Naraoka, 2006) found D-depletion by 33 – 77‰ for both compound classes. Most of that D-depletion occurred between canopy and leaves on the ground (litter), whereas the D-depletion within the litter-soil

profile was only ~5 – 20‰. We find no such systematic directional change, and at SP, we observe that litter is 5 – 15‰ depleted for C_{29} *n*-alkane, but 20 – 30‰ enriched for C_{30} *n*-alkanoic acid relative to average canopy (Fig. 5b). Although it is hard to reconcile the different findings in a Japanese temperate maple forest dominated by just two species (*Acer argutum* and *Acer carpinifolium*) and the Peruvian tropical high biodiversity forest sites spanning an altitude range (this study), one possibility is that there has been a directional change in the hydroclimate at the Japanese location during the time of soil formation. Another possibility is that high biodiversity at our Peruvian sites masks any diagenetic changes, with variability down-profile driven primarily by different species inputs over time. Future work might study the isotope effects down-profile in a wider range of soil types and ecosystems in order to better constrain plant wax δD values in soil archives.

4.1.6 A systematic shift in plant wax δ^{13}C across between canopy, litter and soil

This study was motivated by the observation of plant wax δ^{13}C offsets between canopy leaves and soils (Feakins et al., 2018). In the current detailed study of leaf litter and soil profiles we confirm that offset and study the progression via more detailed sampling within soil pits. We find a 4 – 6‰ enrichment in both plant wax compounds from litter to deeper soils (Fig. 5). The larger enrichment step happens between the litter and top soil (~2 – 4‰) followed by a smaller change (~2‰) deeper in the soil, and the profiles in plant waxes mirror that of bulk OC. The ^{13}C-depletion in litter relative to canopy leaves at SP (~1‰ for C_{29} *n*-alkane and ~3‰ for C_{30} *n*-alkanoic acid, Fig. 5f) may indicate the addition of relatively ^{13}C-depleted understory leaves (Wu et al., 2017). Up to 2‰ of the down-profile ^{13}C-enrichment may be explained by the more enriched pre-industrial atmospheric CO_2 compared to today due to the Suess effect (Francey et

638 al., 2002; Scripps CO_2 program), if the plant waxes in the deeper soils were entirely pre-
639 industrial. Root inputs cannot explain the enrichment in soils, as the roots are 2 – 4‰ depleted
640 relative to soils (Fig. 5f,h). Plant wax $\delta^{13}C$ entering the soils could have shifted through time if
641 there was a directional change in plant type/composition over the timescale of decades; however
642 this is very unlikely in these pristine highly biodiverse tropical forests (except VC) where no
643 single tree species dominate the landscape. Hence, after accounting for Suess effect, we infer at
644 least ~2 – 4‰ of post-mortem ^{13}C-enrichment of plant waxes within soils which is likely a result
645 of diagenesis.

646 Our profiles corroborate previous studies of a leaf-litter-soil sequence in a Japanese maple forest
647 that found ~2.5 – 4‰ ^{13}C-enrichment between leaf and surface soil (Chikaraishi and Naraoka,
648 2006), and depth profiles of three types of tundra-covered British acid upland soils that found ~2
649 – 4‰ ^{13}C-enrichment of $C_{27\text{-}31}$ *n*-alkanes downwards (Huang et al., 1996). Considering very
650 different settings among the three studies (and the continued Suess effect over recent decades),
651 the ^{13}C-enrichment of plant waxes during soil storage appears to be a common feature across a
652 range of environmental and soil conditions. ^{13}C-enrichment of *n*-alkanes during early diagenesis
653 has also been observed in several litterbag experiments in mid-latitude temperate forests, mostly
654 showing 1 – 2‰ enrichment within 1 – 3 years, likely a result of microbial processes (Nguyen
655 Tu et al., 2004; Wang et al., 2014; Li et al., 2017; Zhang et al., 2017). Our study confirms that
656 direction and trend, and reveals additional change down profile, which could be due to the much
657 longer time scale of soil formation compared to the litterbag experiments. Not only do we find
658 this result for the *n*-alkanes, we also confirm this transition in litter and soil profiles for the *n*-
659 alkanoic acids, which have been less often reported in litterbag degradation experiments.

660 ### 4.2 Implications for plant wax calibration studies for paleoclimate applications

661 #### 4.2.1 Soil-based surveys as integrators of plant signals

662 Much attention for modern plant wax studies has focused on leaves from living plants (as
663 summarized in review papers by Sachse et al., 2012; Diefendorf & Freimuth, 2017), but soil-
664 based studies (e.g. Jia et al., 2008) provide integrated records of multi-species plant inputs and
665 post-mortem soil processes that may affect plant wax signatures in the transition from leaf to soil
666 (Nguyen Tu et al., 2004; Chikaraishi & Naraoka, 2006). Several studies have surveyed soils
667 across environmental transects using soils to understand molecular abundance distribution (Bush
668 & McInerney, 2015), carbon isotopic composition (Wei & Jia, 2009; Schwab et al., 2015;
669 Feakins et al., 2018) and hydrogen isotopic composition (e.g. Jia et al., 2008; Bai et al., 2011;
670 Zhang & Liu, 2011; Ernst et al., 2013; Ponton et al., 2014; Zhuang et al., 2015; Nieto-Moreno et
671 al., 2016; Wang et al., 2017; Feakins et al., 2018), almost all of which studied *n*-alkanes, with
672 only few exceptions that have studied *n*-alkanoic acids (Ponton et al., 2014; Feakins et al., 2018;
673 Bakkelund et al., 2018). Although both plant and soil-based approaches have merits, plant-based
674 calibrations include significant scatter among individual plants associated with differences in
675 plant type, species, biosynthetic processes, seasonality and microclimate, whereas soils provide
676 an average of plant inputs and reveal how environmental controls are represented in the soil
677 archive. For example, along a slope of Mount Taibai in China, soil *n*-alkane δD values capture
678 the altitudinal gradient in source water composition which was not observed in plant
679 measurements due to significant scatter among individuals, especially between woody plants and
680 grasses (Zhang & Liu, 2011).

681 Regions of high biodiversity, such as tropical forests, pose even bigger challenges for plant-
682 based calibrations, as large-quantity sampling and knowledge of species dominance may be

683 required to adequately capture the ecosystem-scale average signatures. Recent surveys of plant
684 wax δD and δ^{13}C in canopy leaves in the same region as this study, along a 3320 m elevation
685 transect in the highly-biodiverse tropical forests of the Peruvian Andes, sampled at an
686 unprecedented scale (>300 samples) and revealed significant scatter among individual tree leaves
687 and species. Despite the scatter these studies could identify a robust altitudinal trend (Feakins et
688 al., 2016a,b; Wu et al., 2017), but one that would have been difficult to reveal without substantial
689 sampling of leaves and sites as demonstrated by Monte Carlo simulations (Wu et al., 2017). In
690 contrast, a relatively small number of soil samples may be needed to calibrate the archived proxy
691 across an environmental transect (e.g., as shown for this region in Ponton et al., 2014 and
692 Feakins et al., 2018). In a series of studies in this region, we have both constrained the isotopic
693 signal fixed in the plant canopy (Feakins et al., 2016a,b; Wu et al., 2017), the processes of
694 alteration down profile (this study) and the archived proxy in soils (Ponton et al., 2014; Feakins
695 et al., 2018).

696 Another advantage of soil-based calibrations is that these capture the post-mortem alterations to
697 plant wax signatures during residence in soil, which may modify the environmental information
698 being recorded from time of synthesis. While we find that δD does not systematically vary, we
699 find a 4 – 6‰ ^{13}C-enrichment in both plant wax compounds from litter to deeper soils (Fig. 5).
700 The larger enrichment step happens between the litter and top soil (~2 – 4‰) followed by a
701 smaller change (~2‰) deeper in the soil, and the profiles in plant waxes mirror that of bulk OC.
702 Knowing this, what are the implications for application of plant-based calibrations to the
703 sedimentary record? Corrections for the changing δ^{13}C values of atmospheric CO_2 (Suess effect)
704 based on the year of plant collection can be readily applied, when using modern plant-based
705 calibrations for interpretations of the pre-industrial geologic record. Corrections associated with

706 diagenetic processes in soils will be harder to quantify and we anticipate that the diagenetic
707 effect will likely vary with climate, soil type and microbial community. Based on this study of
708 tropical forests, a 2 – 4‰ diagenetic correction may be relevant for vegetation reconstructions in
709 tropical settings based on soils, paleosols, and sedimentary archives where plant waxes are
710 mainly derived from pre-aged plant waxes that have been diagenetically altered in soils. In
711 contrast, archives that mainly integrate leaves that did not go through soil storage (e.g. swamps,
712 some lakes) may not experience such diagenetic effects.

713 Without a diagenetic correction for soil-stored plant waxes, the reconstruction of vegetation
714 composition using soil-derived plant wax $\delta^{13}C$ may be subject to bias relative to calibrations
715 based on living plants. For example, a common tropical application of carbon isotopic analyses is
716 to estimate the proportion of plants using the C4 pathway (e.g., Schefuß et al., 2003, Castaneda
717 et al., 2009). Based on our C3 tropical forest soils, a 3‰ post-mortem diagenetic enrichment
718 would lead to a ~20% overestimation of C4 coverage (based on a 14‰ difference between C3
719 and C4 end-members in Cerling et al., 1997). Although our study shows a relatively consistent
720 magnitude of ^{13}C-enrichment across a range of elevation and forest types (tropical rain forest,
721 bamboo forest, montane cloud forest), it is likely that the diagenetic isotope effect may vary with
722 climate, soil and ecosystem (e.g. Arctic tundra vs. tropical savanna) as diagenetic changes are
723 likely controlled by various biologic and environmental factors (e.g., leaf structure, temperature,
724 soil porosity, soil wetness and microbial community). Further studies would ideally characterize
725 diagenetic alteration of plant wax in a broad range of *in situ* soil profiles (ideally with age
726 information) and controlled experimental studies of individual variables.

727 4.2.2 Soils, not plants, are the major stock of plant wax

728 We posit that soils are the dominant plant wax stock relative to plant biomass in these tropical
729 forest ecosystems. This inference comes from our estimates of the stock of plant waxes in plants
730 vs soils (Appendix A), explained as follows and calculated along a series of tropical rainforest
731 (TR) and tropical montane cloud forest (TMCF) sites across the same Andes-Amazon transect
732 that were previously studied for plant wax work (Ponton et al., 2014; Feakins et al., 2016a,b; Wu
733 et al., 2017) and are analogous to those studied in more detailed here.

734 To estimate plant wax stock in the leaves of living trees, we take the OC-normalized plant wax
735 concentration data from prior studies (Feakins et al., 2016a,b) multiplied by leaf net primary
736 productivity NPP_{leaf} (Malhi et al. 2016) and average leaf lifespan (1 yr in tropical rainforest and 3
737 yr in tropical montane cloud forest sites; Girardin et al., 2014; Huaraca Huasco et al., 2014) to
738 estimate plant wax stock in the leaves. We estimate that plant wax stock ranges from 0.06 – 1
739 Mg km^{-2} for C_{23-33} *n*-alkanes, and from 0.03 – 0.52 Mg km^{-2} for C_{22-32} *n*-alkanoic acids, with a
740 tendency towards greater stocks of plant waxes on living plants in the TMCF sites.

741 We estimate plant wax stock in soils for the top 30 cm of soils only, using a two-layer (organic
742 and mineral layer) approach, based on OC-normalized plant wax concentration data (Feakins et
743 al., 2018) and soil OC stock estimates (Girardin et al., 2014). We find an estimated 0.6 – 3.9 Mg
744 km^{-2} for *n*-alkanes and 3.2 – 21.5 Mg km^{-2} for *n*-alkanoic acids for the top 30 cm of soils again
745 with a tendency towards bigger stocks in the TMCF. Together these results show a much bigger
746 plant wax stock in soils compared to canopy, which accounts for only 17% and 23% of total *n*-
747 alkane stock, and 1% and 5% of total *n*-alkanoic acid stock, on average for TR and TMCF sites
748 respectively (Fig. 9).

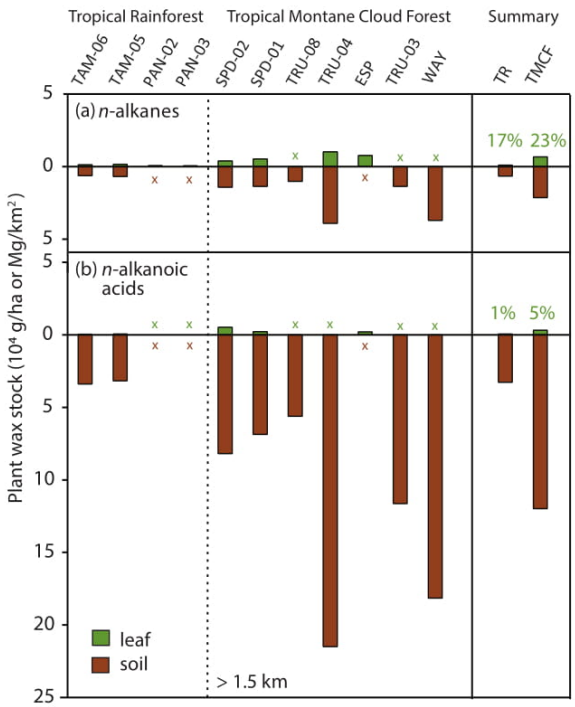

749

750 Fig. 9. Estimates of the stock of plant waxes for (a) $C_{23\text{-}33}$ *n*-alkanes (b) $C_{22\text{-}32}$ *n*-alkanoic acids in leaves (green) and
751 soil top 30cm (brown) across the Peruvian Andes-Amazon elevation transect (sites are ordered in increasing
752 elevation). Plant wax stock in leaves is calculated based on OC-normalized plant wax concentration data (Feakins et
753 al., 2016a,b) multiplied by leaf net primary productivity NPP_{leaf} (Malhi et al., 2016) and then leaf lifespan, using 1 yr
754 in tropical rainforest (TR) sites, and 3 yr in tropical montane cloud forest (TMCF) sites (Girardin et al., 2014;
755 Huaraca Huasco et al., 2014). Soil wax stock is estimated based on OC-normalized plant wax concentration data
756 from soil organic and mineral layers (Feakins et al., 2018) and OC stock estimates for the top 30cm of soils
757 (Girardin et al., 2014). The average of TR and TMCF sites is shown in the summary, with numbers in green
758 indicating the fraction of plant wax stock allocated to the leaves. Crosses denote where leaf or soil estimate is
759 unavailable for the site. Readers are referred to previous publications (Wu et al., 2017, Feakins et al., 2018) for site
760 information.

761 While these estimates are subject to caveats such as not accounting for non-leaf plant waxes in
762 living biomass, and simplification of the two-layer model for soil (top 30 cm) estimates, they
763 depict an overall picture that the vast majority of terrestrial plant waxes is stored in the soils
764 rather than in the living biomass. Moreover, the soil top 30 cm stock represents an
765 underestimation of the overall soil stock, especially in the higher-elevation sites where the
766 organic layers are deeper (Table 1) and plant wax loss with depth is gentler (Fig. 7). Although it
767 has long been known that soils are important archives of OC (Blair et al., 2004), the effort to
768 quantify plant wax production (Feakins et al., 2016a) and here to quantify and compare plant

769 waxes stocks above and below ground, is a new contribution. It would be interesting for carbon
770 cycle quantification and tracking to see this biomarker approach to stocks and fluxes expanded to
771 more climates and ecosystems.

772 #### 4.2.3 Soil stocks as sources for fluvial erosion

773 Given the much greater stock of plant waxes in soils relative to living plants (Fig. 9), soils are the
774 likely source for the majority of riverine-erosion and export of plant waxes used in studies of
775 catchment sourcing (e.g. Ponton et al., 2014; Häggi et al., 2016; Hemingway et al., 2016), and
776 thus for the plant waxes deposited downstream in sedimentary repositories used for paleoclimate
777 reconstructions (e.g., Tipple and Pagani, 2010; Schefuß et al., 2011; Hein et al., 2017). We
778 acknowledge that the actual sourcing from plants vs soils depends not just on the stock, but also
779 on the erosional processes. For example, it has been suggested that landsliding plays an
780 important role in soil OC sourcing to rivers in the Peruvian Andes, stripping 80% of the OC from
781 soils and 20% from vegetation (Clark et al., 2016). Landslides would enhance supply of soil
782 plant waxes from deeper depths (beyond 30 cm), as well as the plant waxes directly from the
783 living biomass. While estimating the exact living vegetation vs soil plant wax sourcing is beyond
784 the scope of this study, we suggest that the stock estimates gives us a first-order view on the
785 relative importance of these two pools, such that soil-based calibrations carry merit of likely
786 being the pool from which most riverine plant waxes are sourced. In terms of parsing fluvial
787 sourcing proportions between living plants and soil stocks of plant wax, compound specific
788 radiocarbon analysis is needed (French et al., 2018).

789 The idea that soil is the major source of sedimentary and riverine plant waxes has important
790 implications especially for elevation-sourcing studies. For example, Feakins et al. (2018)

evaluated fluvial sourcing of plant waxes within the Andes-Amazon Madre de Dios catchment based on plant wax isotopic gradients in soils. If the $\delta^{13}C$ gradient in canopy leaves (which is c. -1 and -2‰ offset from soil organic and mineral layer respectively) were to be used instead, this would result in an overestimate of the average sourcing elevation by more than 700 m (taking *c*.1.5‰ km^{-1} altitudinal gradient for C_{29} *n*-alkane; Feakins et al., 2018). The degree of litter-to-soil ^{13}C-enrichment, however, appears similar across the four sites that span a range in elevation (286 – 3025 m), forest structure (from montane cloud forests to lowland tropical rain forests), and soil organic content (soil organic layer 1 – 26 cm thick, thinner towards lower elevation), such that the $\delta^{13}C$ altitudinal gradients are kept nearly constant between plant and soil, though their values may be offset (Feakins et al., 2018). This implies that when relative isotopic changes are interpreted (e.g., as relative shifts in C3/C4 coverage, or when applying $\delta^{13}C$ in plant waxes for paleoaltimetry reconstruction) instead of the absolute values, the problem caused by ^{13}C-enrichment within soils may be avoided.

5. Conclusions

Here we studied plant wax biomarkers (*n*-alkanes and *n*-alkanoic acids) from four locations (six soil pits) along a 2740 m elevation transect in the Andes-Amazon. We measured plant wax concentrations, molecular distributions, and hydrogen and carbon isotopic compositions, as well as bulk organic carbon and carbon isotopic composition, in these litter-soil profiles. Based on the observations within these profiles we draw inferences about inputs, degradation processes and alteration of plant wax properties within these tropical soil profiles. Within leaf litter, although both compound classes decline in absolute abundance, we find that *n*-alkanes are lost relative to *n*-alkanoic acids, and it is this greater loss of *n*-alkanes (rather than in-soil inputs of *n*-alkanoic

acids) which leads to an increase in *n*-alkanoic acid relative abundance from litter to soil. Within the soil profiles, concentrations of both compound classes decline with depth (k_z) at similar rates within a site. Between sites, k_z decreases with elevation, such that k_z is smaller at higher elevation (colder) sites and larger at lowland (warmer) sites. The only exception to this trend is at VC, the only soil sampled under a secondary growth forest, now dominated by bamboo, and aspects of the disturbance history or bamboo regrowth may explain the lower than expected k_z. We find signs of microbial activities altering molecular distributions of plant waxes, but no evidence of root and fungal contributions being quantitatively important. Across the litter-soil profiles, we find no systematic change in δD values, but a consistent 4 – 6‰ increase in δ^{13}C down-profile, which is attributed to a combination of Suess effect (≤2‰) and diagenetic processes (2 – 4‰), corroborating results from previous litter degradation experiments. With these observations, we suggest that soil-based calibrations carry considerable merit as integrated recorder of plant signals, and this approach is especially relevant in high biodiversity ecosystems where it reduces the number of samples needed to adequately characterize the system. Further, soil-based calibrations capture the post-mortem diagenetic processes that affect plant wax. It is important to characterize plant waxes in soils for a range of applications. Most obviously, surveying plant waxes within modern soil profiles is important for calibration of the recorded signals that may inform applications to paleosol archives of the plant wax proxy. As we show the below-ground stock of plant wax is much greater than that of the living forest here, further quantification and characterization of the soil stock of plant waxes in a range of environments and ecosystems would be informative for carbon cycle and sourcing studies. While not all soils are connected to fluvial systems, some soils are episodically eroded in this system by landslides in high relief areas and by migrating river meanders in lowland systems. Overall, river studies of

plant wax export have shown that soil storage contributes pre-aged plant waxes to the export flux, although to variable extent in different climates and river systems (Kusch et al., 2010; Feng et al., 2015; French et al., 2018). We therefore encourage further modern soil-surveys of plant waxes to understand the exported signal of eroded soils and plant waxes for carbon cycle implications, and when deposited in sedimentary archives, for paleoclimate reconstructions.

Acknowledgements

This material is based upon work supported by the US National Science Foundation under Grant Nos. EAR-1455352 to A.J.W. and EAR-1703141 to S.J.F. In Perú, we thank the Servicio Nacional de Áreas Naturales Protegidas por el Estado (SERNANP) for logistical assistance and permission to work in the protected areas. We thank the Amazon Conservation Association for use of the Wayqecha, Villa Carmen, and CICRA-Los Amigos Research Stations, and for help with field logistics, as well as the Andes Biodiversity and Ecosystems Research Group ABERG (andesresearch.org). Soil pits were dug, described and sampled by the USC GEOL 465 class of 2016, with thanks especially to A. Figueroa, K. Morales and K. O'Rourke. We thank Nick Rollins for laboratory assistance. We thank the Associate Editor Philip Meyers and the reviewers (Aaron Diefendorf, Rencheng Li, and an anonymous reviewer) for their thoughtful comments that helped improve this manuscript.

Appendix A. Supplementary material

Supplementary data associated with this article can be found, in the online version, at https://doi.org/10.101x/j.orggeochem.2019.xx.xxx. These data include an Excel file of all the data, as well as Google maps of the most important areas described in this article.

Data are permanently archived at Pangaea and can be downloaded from

https://doi.pangaea.de/10.1594/PANGAEA.895994.

References

Amundson, R., 2014. Soil Formation, In: Treatise on Geochemistry (Second Edition). Elsevier, Oxford, pp. 1–26.

Bai, Y., Fang, X., Gleixner, G., & Mügler, I., 2011. Effect of precipitation regime on δD values of soil n-alkanes from elevation gradients – Implications for the study of paleo-elevation. Organic Geochemistry 42(7), 838–845.

Bakkelund, A., Porter, T.J., Froese, D.G., Feakins, S.J., 2018. Net fractionation of hydrogen isotopes in *n*-alkanoic acids from soils in the northern boreal forest. Organic Geochemistry 125, 1–13.

Batjes, N. H., 1996. Total carbon and nitrogen in the soils of the world. European Journal of Soil Science 47(2), 151–163.

Blair, N. E., Leithold, E.L., & Aller, R.C., 2004. From bedrock to burial: the evolution of particulate organic carbon across coupled watershed-continental margin systems. Marine Chemistry 92, 141–156.

Brittingham, A., Hren, M. T., & Hartman, G., 2017. Microbial alteration of the hydrogen and carbon isotopic composition of n-alkanes in sediments. Organic Geochemistry 107, 1–8.

Bull, I. D., Bergen, P. F. va., Nott, C. J., Poulton, P. R., & Evershed, R. P., 2000. Organic geochemical studies of soils from the Rothamsted classical experiments—V. The fate of lipids in different long-term experiments. Organic Geochemistry 31(5), 389–408.

Bush, R. T., & McInerney, F. A., 2015. Influence of temperature and C4 abundance on n-alkane chain length distributions across the central USA. Organic Geochemistry 79(0), 65–73.

Castaneda, I. S., Mulitza, S., Schefuß, E., Lopes dos Santos, R. A., Sinninghe Damsté, J. S., Schouten, S., 2009. Wet phases in the Sahara/Sahel region and human migration patterns in North Africa. Proceedings of the National Academy of Sciences 106, 20159–20163.

Cerling, T. E., Harris, J. M., MacFadden, B. J., Leakey, M. G., Quade, J., Eisenmann, V., & Ehleringer, J. R., 1997. Global vegetation change through the Miocene/Pliocene boundary. Nature 389(6647), 153–158.

Cerling, T. E. & Quade, J., 1989. Carbon Isotopes in Paleosol Carbonates as Paleoecologic Indicators. American Journal of Physical Anthropology 78(2), 203–203.

Chikaraishi, Y., & Naraoka, H., 2006. Carbon and hydrogen isotope variation of plant biomarkers in a plant–soil system. Chemical Geology 231(3), 190–202.

Clark, K. E., West, A. J., Hilton, R. G., Asner, G. P., Quesada, C. A., Silman, M. R., et al., 2016. Storm-triggered landslides in the Peruvian Andes and implications for topography, carbon cycles, and biodiversity. Earth Surface Dynamamics 4(1), 47–70.

Dexter, K.G., Lavin, M., Torke, B.M., Twyford, A.D., Kursar, T.A., Coley, P.D., Drake, C., Hollands, R., Pennington, R.T., 2017. Dispersal assembly of rain forest tree communities across the Amazon basin. Proceedings of the National Academy of Sciences 114, 2645-2650.

892 Diefendorf, A. F., & Freimuth, E. J., 2017. Extracting the most from terrestrial plant-derived n-alkyl lipids and their
893 carbon isotopes from the sedimentary record: A review. Organic Geochemistry 103, 1–21.

894 Eglinton, G., & Hamilton, R. J., 1967. Leaf Epicuticular Waxes. Science 156(3780), 1322.

895 Eglinton, T. I., & Eglinton, G., 2008. Molecular proxies for paleoclimatology. Earth and Planetary Science Letters
896 275(1), 1–16.

897 Ernst, N., Peterse, F., Breitenbach, S. F. M., Syiemlieh, H. J., & Eglinton, T. I., 2013. Biomarkers record
898 environmental changes along an altitudinal transect in the wettest place on Earth. Organic Geochemistry
899 60, 93–99.

900 Feakins, S. J., & Sessions, A. L., 2010. Controls on the D/H ratios of plant leaf waxes in an arid ecosystem.
901 Geochimica et Cosmochimica Acta 74(7), 2128–2141.

902 Feakins, S. J., Bentley, L. P., Salinas, N., Shenkin, A., Blonder, B., Goldsmith, G. R., et al., 2016a. Plant leaf wax
903 biomarkers capture gradients in hydrogen isotopes of precipitation from the Andes and Amazon.
904 Geochimica et Cosmochimica Acta 182, 155–172.

905 Feakins, S. J., Peters, T., Wu, M. S., Shenkin, A., Salinas, N., Girardin, C. A. J., et al., 2016b. Production of leaf
906 wax n-alkanes across a tropical forest elevation transect. Organic Geochemistry 100, 89–100.

907 Feakins, S. J., Wu, M. S., Ponton, C., Galy, V., & West, A.J., 2018. Dual isotope evidence for uniform sedimentary
908 integration of plant wax biomarkers across an Andes-Amazon elevation transect. Geochimica et
909 Cosmochimica Acta, doi:10.1016/j.gca.2018.09.007.

910 Feng, X., Gustafsson, Ö., Holmes, R.M., Vonk, J.E., Dongen, B.E., Semiletov, I.P., Dudarev, O.V., Yunker, M.B.,
911 Macdonald, R.W., Wacker, L., Montluçon, D.B., Eglinton, T.I., 2015. Multimolecular tracers of terrestrial
912 carbon transfer across the pan-Arctic: 14C characteristics of sedimentary carbon components and their
913 environmental controls. Global Biogeochemical Cycles 29, 1855–1873.

914 Feng, X., Feakins, S. J., Liu, Z., Ponton, C., Wang, R. Z., Karkabi, E., et al., 2016. Source to sink: Evolution of
915 lignin composition in the Madre de Dios River system with connection to the Amazon basin and offshore.
916 Journal of Geophysical Research: Biogeosciences 121(5), 1316–1338.

917 Fornace, K., Hughen, K. A., Shanahan, T. M., Fritz, S. C., Baker, P.A ., & Sylva, S. P., 2014. A 60,000-year record
918 of hydrologic variability in the Central Andes from the hydrogen isotopic composition of leaf waxes in
919 Lake Titicaca sediments. Earth and Planetary Science Letters 408(0), 263–271.

920 Francey R. J., Allison C. E., Etheridge D. M., Trudinger C. M., Enting I. G., Leuenberger M., et al., 2002. A
921 1000-year high precision record of $\delta^{13}C$ in atmospheric CO_2. Tellus B 51(2), 170–193.

922 French, K. L., Hein, C. J., Haghipour, N., Wacker, L., Kudrass, H. R., Eglinton, T. I., & Galy, V., 2018. Millennial
923 soil retention of terrestrial organic matter deposited in the Bengal Fan. Scientific Reports 8(1), 11997.

924 Häggi, C., Sawakuchi, A. O., Chiessi, C. M., Mulitza, S., Mollenhauer, G., Sawakuchi, H. O., et al., 2016. Origin,
925 transport and deposition of leaf-wax biomarkers in the Amazon Basin and the adjacent Atlantic.
926 Geochimica et Cosmochimica Acta 192, 149–165.

927 Heimsath, A. M., Dietrich, W. E., Nishiizumi, K., & Finkel, R. C., 1997. The soil production function and landscape
928 equilibrium. Nature 388, 358.

929 Hein, C. J., Galy, V., Galy, A., France-Lanord, C., Kudrass, H., Schwenk, T., 2017. Post-glacial climate forcing of
930 surface processes in the Ganges-Brahmaputra river basin and implications for carbon sequestration. Earth
931 and Planetary Science Letters 478, 89–101.

Hemingway, J. D., Schefuß, E., Dinga, B. J., Pryer, H., & Galy, V. V., 2016. Multiple plant-wax compounds record differential sources and ecosystem structure in large river catchments. Geochimica et Cosmochimica Acta 184, 20–40.

Hoffmann, B., Feakins, S. J., Bookhagen, B., Olen, S. M., Adhikari, D. P., Mainali, J., & Sachse, D., 2016. Climatic and geomorphic drivers of plant organic matter transport in the Arun River, E Nepal. Earth and Planetary Science Letters 452, 104–114

Huang, Y., Eglinton, G., Ineson, P., Latter, P. M., Bol, R., & Harkness, D. D., 1997. Absence of carbon isotope fractionation of individual n-alkanes in a 23-year field decomposition experiment with Calluna vulgaris. Organic Geochemistry 26(7), 497–501.

Huang, Yongsong, Bol, R., Harkness, D. D., Ineson, P., & Eglinton, G., 1996. Post-glacial variations in distributions, 13C and 14C contents of aliphatic hydrocarbons and bulk organic matter in three types of British acid upland soils. Organic Geochemistry 24(3), 273–287.

Ji, Y., Mao, G., Wang, Y., & Bartlam, M., 2013. Structural insights into diversity and n-alkane biodegradation mechanisms of alkane hydroxylases. Frontiers in Microbiology 4, 58.

Jia, G., Wei, K., Chen, F., & Peng, P., 2008. Soil n-alkane δD vs. altitude gradients along Mount Gongga, China. Geochimica et Cosmochimica Acta 72(21), 5165–5174

Jobbágy Esteban G., & Jackson Robert B., 2000. The vertical distribution of soil organic carbon and its relation to climate and vegetation. Ecological Applications 10(2), 423–436.

Kögel-Knabner, I., & Amelung, W., 2014. Dynamics, Chemistry, and Preservation of Organic Matter in Soils, In: Treatise on Geochemistry (Second Edition). Elsevier, Oxford, pp. 157–215.

Kusch, S., Rethemeyer, J., Schefuß, E., & Mollenhauer, G., 2010. Controls on the age of vascular plant biomarkers in Black Sea sediments. Geochimica et Cosmochimica Acta 74, 7031-7047.

Li, G., Li, L., Tarozo, R., Longo, W. M., Wang, K. J., Dong, H., & Huang, Y., 2018. Microbial production of long-chain n-alkanes: Implication for interpreting sedimentary leaf wax signals. Organic Geochemistry 115, 24–31.

Li, R., Luo, G., Meyers, P. A., Gu, Y., Wang, H., & Xie, S., 2012. Leaf wax n-alkane chemotaxonomy of bamboo from a tropical rain forest in Southwest China. Plant Systematics and Evolution 298(4), 731–738.

Li, R., Meyers, P. A., Fan, J., & Xue, J., 2016. Monthly changes in chain length distributions and stable carbon isotope composition of leaf n-alkanes during growth of the bamboo Dendrocalamus ronganensis and the grass Setaria viridis. Organic Geochemistry 101, 72–81.

Li, R., Fan, J., Xue, J., & Meyers, P. A., 2017. Effects of early diagenesis on molecular distributions and carbon isotopic compositions of leaf wax long chain biomarker n-alkanes: Comparison of two one-year-long burial experiments. Organic Geochemistry 104, 8–18.

Liu, W., Fox, J. E. D., & Xu, Z., 2000. Leaf litter decomposition of canopy trees, bamboo and moss in a montane moist evergreen broad-leaved forest on Ailao Mountain, Yunnan, south-west China. Ecological Research 15(4), 435–447.

Madan, R., Pankhurst, C., Hawke, B., & Smith, S., 2002. Use of fatty acids for identification of AM fungi and estimation of the biomass of AM spores in soil. Soil Biology and Biochemistry 34(1), 125–128.

970 Magill, C. R., Ashley, G. M., Dominguez-Rodrigo, M., & Freeman, K. H., 2016. Dietary options and behavior
971 suggested by plant biomarker evidence in an early human habitat. Proceedings of the National Academy of
972 Sciences 113(11), 2874–2879.

973 Makou M., Eglinton T., McIntyre C., Montluçon D., Antheaume I., & Grossi V., 2018. Plant Wax n-Alkane and
974 n-Alkanoic Acid Signatures Overprinted by Microbial Contributions and Old Carbon in Meromictic Lake
975 Sediments. Geophysical Research Letters 45(2), 1049–1057.

976 Marseille F., Disnar J. R., Guillet B., & Noack Y., 1999. n-Alkanes and free fatty acids in humus and A1 horizons of
977 soils under beech, spruce and grass in the Massif-Central (Mont-Lozère), France. European Journal of Soil
978 Science 50(3), 433–441.

979 Naafs, D. F. ., van Bergen, P. F., Boogert, S. J., & de Leeuw, J. W., 2004. Solvent-extractable lipids in an acid andic
980 forest soil; variations with depth and season. Soil Biology and Biochemistry 36(2), 297–308.

981 Nguyen Tu, T.T., Egasse, C., Zeller, B., Bardoux, G., Biron, P., Ponge, J.-F., et al., 2011. Early degradation of plant
982 alkanes in soils: A litterbag experiment using 13C-labelled leaves. Soil Biology and Biochemistry 43(11),
983 2222–2228.

984 Nguyen Tu, T.T., Egasse, C., Anquetil, C., Zanetti, F., Zeller, B., Huon, S., & Derenne, S., 2017. Leaf lipid
985 degradation in soils and surface sediments: A litterbag experiment. Organic Geochemistry 104, 35–41.

986 Nguyen Tu, T.T, Derenne, S., Largeau, C., Bardoux, G., & Mariotti, A., 2004. Diagenesis effects on specific carbon
987 isotope composition of plant n-alkanes. Selected Papers from the Eleventh International Humic Substances
988 Society Conference 35(3), 317–329.

989 Nieto-Moreno, V., Rohrmann, A., van der Meer, M. T. J., Sinninghe Damsté, J. S., Sachse, D., Tofelde, S., et al.,
990 2016. Elevation-dependent changes in n-alkane δD and soil GDGTs across the South Central Andes. Earth
991 and Planetary Science Letters 453, 234–242.

992 Nottingham, A. T., Whitaker, J., Turner, B. L., Salinas, N., Zimmermann, M., Malhi, Y., & Meir, P., 2015. Climate
993 Warming and Soil Carbon in Tropical Forests: Insights from an Elevation Gradient in the Peruvian Andes.
994 BioScience 65(9), 906–921.

995 Oades, J. M., 1993. The role of biology in the formation, stabilization and degradation of soil structure. International
996 Workshop on Methods of Research on Soil Structure/Soil Biota Interrelationships 56(1), 377–400.

997 Piperno, D. R. and D. M. Pearsall., 1998. The silica bodies of tropical American grasses: Morphology, taxonomy,
998 and implications for grass systematics and fossil phytolith identification. Smithsonian Contributions to
999 Botany 85:1–40.

1000 Pitman, N.C.A., Terborgh, J.W., Silman, M.R., Núñez, V.P., Neill, D.A., Cerón, C.E., Palacios, W.A. and Aulestia,
1001 M., 2001. Dominance and distribution of tree species in upper Amazonian terra firme forests. Ecology
1002 82(8), 2101–2117.

1003 Ponton, C., West, A. J., Feakins, S. J., & Galy, V., 2014. Leaf wax biomarkers in transit record river catchment
1004 composition. Geophysical Research Letters 41(18), 6420–6427.

1005 Quade, J., Eiler, J., Daëron, M., & Achyuthan, H., 2013. The clumped isotope geothermometer in soil and paleosol
1006 carbonate. Geochimica Et Cosmochimica Acta 105, 92–107.

1007 Rasse, D. P., Rumpel, C., & Dignac, M.-F., 2005. Is soil carbon mostly root carbon? Mechanisms for a specific
1008 stabilisation. Plant and Soil 269(1), 341–35

1009 Retallack, G. J., 2013. Global cooling by grassland soils of the geological past and near future. Annual Review of
1010 Earth and Planetary Sciences 41, 69-86.

1011 Rommerskirchen F., Eglinton G., Dupont L., Güntner U., Wenzel C., & Rullkötter J., 2003. A north to south transect
1012 of Holocene southeast Atlantic continental margin sediments: Relationship between aerosol transport and
1013 compound-specific δ13C land plant biomarker and pollen records. Geochemistry, Geophysics, Geosystems,
1014 4(12). https://doi.org/10.1029/2003GC000541

1015 Sachse, D., Radke, J., & Gleixner, G., 2004. Hydrogen isotope ratios of recent lacustrine sedimentary n-alkanes
1016 record modern climate variability. Geochimica et Cosmochimica Acta 68(23), 4877–4889.

1017 Sachse, D., Billault, I., Bowen, G. J., Chikaraishi, Y., Dawson, T. E., Feakins, S. J., et al., 2012. Molecular
1018 Paleohydrology: Interpreting the Hydrogen-Isotopic Composition of Lipid Biomarkers from
1019 Photosynthesizing Organisms. Annual Review of Earth and Planetary Sciences 40(1), 221–249.

1020 Salinas N., Malhi Y., Meir P., Silman M., Roman Cuesta R., Huaman J., et al., 2010. The sensitivity of tropical leaf
1021 litter decomposition to temperature: results from a large-scale leaf translocation experiment along an
1022 elevation gradient in Peruvian forests. New Phytologist 189(4), 967–977.

1023 Schefuß, E., Schouten, S., Jansen, J. H. F., Sinninghe Damsté, J. S., 2003. African vegetation controlled by tropical
1024 sea surface temperatures in the mid-Pleistocene period. Nature 422, 418–421.

1025 Schefuß, E., Kuhlmann, H., Mollenhauer, G., Prange, M., Pätzold, J., 2011. Forcing of wet phases in southeast
1026 Africa over the past 17,000 years. Nature 480, 509–512.

1027 Schmidt, M. W. I., Torn, M. S., Abiven, S., Dittmar, T., Guggenberger, G., Janssens, I. A., et al., 2011. Persistence
1028 of soil organic matter as an ecosystem property. Nature 478, 49.

1029 Schwab, V. F., Garcin, Y., Sachse, D., Todou, G., Séné, O., Onana, J.-M., et al., 2015. Effect of aridity on δ13C and
1030 δD values of C3 plant- and C4 graminoid-derived leaf wax lipids from soils along an environmental
1031 gradient in Cameroon (Western Central Africa). Organic Geochemistry 78, 99–109.

1032 Scripps CO2 program. "Mauna Loa and South Pole Isotopic ^{13}C Ratio".
1033 http://scrippsco2.ucsd.edu/graphics_gallery/isotopic_data/mauna_loa_and_south_pole_isotopic_c13_ratio
1034 (accessed May 2018)

1035 Silman, M. R., 2014. Functional megadiversity. Proceedings of the National Academy of Sciences 111(16), 5763.

1036 Summons R. E., Bird L. R., Gillespie A. L., Pruss S. B., Roberts M., & Sessions A. L., 2013. Lipid biomarkers in
1037 ooids from different locations and ages: evidence for a common bacterial flora. Geobiology 11(5), 420–
1038 436.

1039 Tipple, B. K., & Pagani, M., 2010. A 35 Myr North American leaf-wax compound-specific carbon and hydrogen
1040 isotope record: Implications for C4 grasslands and hydrologic cycle dynamics. Earth and Planetary Science
1041 Letters 299(1-2), 250-262.

1042 Torres, M. A., Limaye, A. B., Ganti, V., Lamb, M. P., West, A. J., & Fischer, W. W. 2017. Model predictions of
1043 long-lived storage of organic carbon in river deposits. Earth Surface Dynamics 5(4), 711-730.

1044 Vogts, A., Moossen, H., Rommerskirchen, F., & Rullkötter, J., 2009. Distribution patterns and stable carbon isotopic
1045 composition of alkanes and alkan-1-ols from plant waxes of African rain forest and savanna {C3} species.
1046 Organic Geochemistry 40(10), 1037–105

1047 Wang, C., Hren, M. T., Hoke, G. D., Liu-Zeng, J., & Garzione, C. N., 2017. Soil n-alkane δD and glycerol dialkyl
1048 glycerol tetraether (GDGT) distributions along an altitudinal transect from southwest China: Evaluating
1049 organic molecular proxies for paleoclimate and paleoelevation. Organic Geochemistry 107, 21–32.

1050 Wang, G., Zhang, L., Zhang, X., Wang, Y., & Xu, Y., 2014. Chemical and carbon isotopic dynamics of grass
1051 organic matter during litter decompositions: A litterbag experiment. Organic Geochemistry 69, 106–113.

1052 Weete, J. D., 1972. Aliphatic hydrocarbons of the fungi. Phytochemistry 11(4), 1201–1205.

1053 Wei, K., & Jia, G., 2009. Soil n-alkane δ13C along a mountain slope as an integrator of altitude effect on plant
1054 species δ13C. Geophysical Research Letters, 36(11), https://doi.org/10.1029/2009GL038294

1055 Whitaker Jeanette, Ostle Nicholas, Nottingham Andrew T., Ccahuana Adan, Salinas Norma, Bardgett Richard D., et
1056 al., 2014. Microbial community composition explains soil respiration responses to changing carbon inputs
1057 along an Andes-to-Amazon elevation gradient. Journal of Ecology 102(4), 1058–1071.

1058 Wiesenberg, G. L. B., Schneckenberger, K., Schwark, L., & Kuzyakov, Y., 2012. Use of molecular ratios to identify
1059 changes in fatty acid composition of Miscanthus×giganteus (Greef et Deu.) plant tissue, rhizosphere and
1060 root-free soil during a laboratory experiment. Organic Geochemistry 46, 1–11.

1061 Wilkie, K. M. K., Chapligin, B., Meyer, H., Burns, S., Petsch, S., & Brigham-Grette, J., 2013. Modern isotope
1062 hydrology and controls on δD of plant leaf waxes at Lake El'gygytgyn, NE Russia. Climate of the Past
1063 9(1), 335–352.

1064 Wu, M. S., Feakins, S. J., Martin, R. E., Shenkin, A., Bentley, L. P., Blonder, B., et al., 2017. Altitude effect on leaf
1065 wax carbon isotopic composition in humid tropical forests. Geochimica et Cosmochimica Acta 206, 1–17.

1066 Yadvinder, M., Girardin C. A. J., Goldsmith G. R., Doughty C. E., Salinas N., Metcalfe D. B., et al., 2016. The
1067 variation of productivity and its allocation along a tropical elevation gradient: a whole carbon budget
1068 perspective. New Phytologist 214(3), 1019–1032.

1069 Zech, M., Pedentchouk, N., Buggle, B., Leiber, K., Kalbitz, K., Marković, S. B., & Glaser, B., 2011. Effect of leaf
1070 litter degradation and seasonality on D/H isotope ratios of n-alkane biomarkers. Geochimica et
1071 Cosmochimica Acta 75(17), 4917–4928.

1072 Zhang, P., & Liu, W., 2011. Effect of plant life form on relationship between δD values of leaf wax n-alkanes and
1073 altitude along Mount Taibai, China. Organic Geochemistry 42(1), 100–107.

1074 Zhang, Y., Zheng, M., Meyers, P. A., & Huang, X., 2017. Impact of early diagenesis on distributions of Sphagnum
1075 n-alkanes in peatlands of the monsoon region of China. Organic Geochemistry 105, 13–19.

1076 Zhou, B., Fu,M., Xie, J., Yang, X., & Li, Z., 2005. Ecological functions of bamboo forest: Research and
1077 Application. Journal of Forestry Research 16, 143–147.

1078 Zhuang, G., Pagani, M., Chamberlin, C., Strong, D., & Vandergoes, M., 2015. Altitudinal shift in stable hydrogen
1079 isotopes and microbial tetraether distribution in soils from the Southern Alps, NZ: Implications for
1080 paleoclimatology and paleoaltimetry. Organic Geochemistry 79, 56–64.

Figure Captions

Fig. 1. Sampling locations across a 2740 m elevation Andes-Amazon transect in the Cusco and Madre de Dios region of Peru (square symbols, color indicates elevation). Andean sites: Wayqecha (WAY) and San Pedro (SP). Foothills: Villa Carmen (VC) Lowland: Los Amigos (LA). Circles show major cities in the region.

Fig. 2. Vertical profiles of plant wax and bulk OC abundance at the four study sites (pink: C_{23-33} *n*-alkanes; blue: C_{22-32} *n*-alkanoic acids), showing (a-d) total organic carbon concentrations, (e-h) abundance per gram dry weight (∑alk and ∑acid), (i-l) abundance normalized to OC (Λalk and Λacid), (m-p) *n*-alkanoic acid fraction. Data shown are from this study (litter: triangle; root: inverted triangle; soil: square), as well as from previous studies (canopy: diamond; soil: circle) of overlapping sites at WAY and SP (Feakins et al. 2016a,b; Feakins et al., 2018). Open symbols at LA and VC denote additional pits at these sites at the ridge top, with closed symbols representing slope base. Vertical bars indicate the depth range from which the soil profile samples were taken. Horizontal bars of canopy data at SP represent standard error of the site means (n = 39). Note the change in x-axes for soil data on the left panels.

Fig. 3. Chain length distributions of *n*-alkanes (left) and *n*-alkanoic acids (right) in litter (green), soil (yellow), and root (purple) at the four study sites. Error bars represent 1σ deviation from the mean values when multiple litter or soil samples are present at a single site.

Fig. 4. Vertical profiles of (left) carbon preference index (CPI) and (right) average chain length (ACL) of C_{23-33} *n*-alkanes (pink) and C_{22-32} *n*-alkanoic acids (blue) at the four study sites, showing data from this study (litter: triangle; root: inverted triangle; soil: square). Open symbols at LA and VC denote additional pits at these sites at the ridge top, with closed symbols representing slope base. Also shown are canopy (diamond) and soil (circle) data from previous studies of overlapping sites at WAY and SP (Feakins et al. 2016a,b; Feakins et al., 2018). Vertical bars indicate the depth range from which the soil profile samples were taken. Horizontal error bars of canopy data at SP represent standard error of the site means (n = 39).

Fig. 5. Vertical profiles of (left, a-d) δD and (right, e-h) δ^{13}C of C_{29} *n*-alkane (pink), C_{30} *n*-alkanoic acid (blue), and bulk OC (grey) at the four study sites, showing data from this study (litter: triangle; root: inverted triangle; soil: square). Open symbols at LA and VC denote additional pits at these sites at the ridge top, with closed symbols representing slope base. Also shown are canopy (diamond) and soil (circle) data from previous studies of overlapping sites at WAY and SP (Feakins et al. 2016a; Wu et al. 2017; Feakins et al., 2018) for comparison. Vertical bars indicate the depth range from which the soil profile samples were taken. Horizontal bars indicate 1σ error from replicate measurements (for soil and litter data) or standard errors of site mean (canopy data at SP).

Fig. 6. Exponential decrease in the total abundance of (a) bulk OC, (b) *n*-alkanes (C_{23-33}), and (c) *n*-alkanoic acids (C_{22-32}) within soils profiles at the four sites. Data show fractional

concentrations relative to the top soil samples at each site. Soil data are plotted on the mean sample depth below the top sample. Depth-dependent rate constants (k_z) are estimated with 1σ uncertainties, which show the same values within uncertainties among compounds, except at for *n*-alkanes WAY and bulk OC at LA. Soil profiles at ridgetop (open symbol) and slope base (solid symbol) at VC are grouped for curve fitting. Note that the ridgetop soil pit at LA is excluded in this analysis due to the very thin soil O layer (1 cm) at much finer resolution than the top sample (0-7 cm).

Fig. 7. The rate of OC and plant wax loss with soil depth (k_z; this study) and litter decomposition rate (k; Salinas et al., 2010) along the Andes-Amazon elevation transect. Note that the soil under secondary growth at VC is an outlier that does not follow the temperature-dependency of k_z values. Litter bag experiments were not conducted at the secondary forest sites at VC. The lower than expected k_z value for bulk OC at LA (the lowest elevation site) may be in part explained by the recalcitrance of residual bulk organic material at depth in these soils.

Fig. 8. Increase in mid-chain ($C_{23\text{-}25}$) *n*-alkane fractional abundance down the litter-soil profiles, showing data from litter (triangles) and soils (squares) from the four sites. Note that both ridgetop (open symbols) and slope base (solid symbols) pits are shown for VC and LA. We find no such consistent increase in mid-chain proportions for *n*-alkanoic acids across the sites.

Fig. 9. Estimates of the stock of plant waxes for (a) $C_{23\text{-}33}$ *n*-alkanes (b) $C_{22\text{-}32}$ *n*-alkanoic acids in leaves (green) and soil top 30cm (brown) across the Peruvian Andes-Amazon elevation transect (sites are ordered in increasing elevation). Plant wax stock in leaves is calculated based on OC-normalized plant wax concentration data (Feakins et al., 2016a,b) multiplied by leaf net primary productivity NPP_{leaf} (Malhi et al., 2016) and then leaf lifespan, using 1 yr in tropical rainforest (TR) sites, and 3 yr in tropical montane cloud forest (TMCF) sites (Girardin et al., 2014; Huaraca Huasco et al., 2014). Soil wax stock is estimated based on OC-normalized plant wax concentration data from soil organic and mineral layers (Feakins et al., 2018) and OC stock estimates for the top 30cm of soils (Girardin et al., 2014). The average of TR and TMCF sites is shown in the summary, with numbers in green indicating the fraction of plant wax stock allocated to the leaves. Crosses denote where leaf or soil estimate is unavailable for the site. Readers are referred to previous publications (Wu et al., 2017, Feakins et al., 2018) for site information.

Highlights:

- Plant wax was studied in soil pits under tropical forests at varied elevation.
- Plant wax concentration and composition were characterized in litter and soil profiles.
- Plant wax D/H invariant within the profiles.
- Significant down-profile ^{13}C-enrichment linked to Suess effect and diagenesis.
- Below-ground plant wax stocks greatly exceed above-ground stocks.